ASSOCIATION EURATOM - UNIVERSITY OF LATVIA

AEUL

ANNUAL REPORT 2010

Riga 2011

TABLE OF CONTENT

1. INTRODUCTION

This Annual Report summarises the fusion research activities of the Latvian Research Unit of the Association EURATOM-University of Latvia in 2010.

There is now general agreement that the economy of the world must be radically transformed in the coming decades, either because fossil fuels become exhausted, or because of environmental concerns relating to emission of CO_2 and other greenhouse gases. In this context, fusion power may come to play a critical role in meeting the energy requirements of the world.

Fusion energy is a safe form of nuclear energy, which does not pollute the atmosphere. The fundamental "fuels" heavy hydrogen (deuterium) and lithium are found abundantly in seawater and in the earth's crust and will provide the world with energy in the many millions of years. The primary waste is the power plant. Power plants become radioactive, but the radioactivity will be gone after 100 years, and there will therefore be no need for long-term storage of waste.

Worldwide coordinated fusion research started in the late 1950s to find ways to use fusion as an energy source here on Earth. In 2006 seven parties, EU, Japan, Russia, China, USA, Korea and India, signed the agreement to build and exploit ITER - International Thermonuclear Experimental Reactor, and to place ITER in Cadarache in France. It is expected that ITER will be ready for scientific exploitation in 2024.

The mission of ITER is to demonstrate that nuclear fusion can be exploited as an energy source. ITER represents an unexpected international cooperation in the field of science and technology. ITER also represents a valuable opportunity for cooperation between public research organisations and private industry.

The principle being pursued with ITER is the fusion of hydrogen isotopes (deuterium and tritium) to form helium. To make the fusion process run at significant rate the hydrogen gas must be heated to high temperatures where it ionises and turns into a plasma. The plasma must be confined to achieve suitable densities and sustain the high temperature. ITER will use a magnetic field for the confinement.

After ITER a prototype commercial power station DEMO will be constructed. DEMO is expected to be operational sometime in the 2030s, so that widespread adoption could occur in mid-century.

The activities of the Research Unit are divided in the Fusion Physics Programme and Technology under the Contract of Association and Technology Programme under

EFDA. The AEUL in the frame of the EFDA Workprogramme 2008 starts to take part in the Goal Oriented Training Programme - GOT "EUROBREED".

The Physics Programme is carried out at IP UL – Institute of Physics, University of Latvia, and at ISSP UL – Institute of Solid State Physics, University of Latvia. The research areas of the Physics Programme are:

- Preparation of a gallium jet limiter for testing under reactor relevant conditions
- Characterization of the impurity concentration, profiling and erosion in ITER relevant materials using *ex situ* LIBS spectroscopy
- *In situ* tokamak laser enhanced LIBS spectroscopy of the impurity concentration depth profile in wall tiles
- Theory and Code Development:

  - On the theory of high-power gyrotrons with uptapered resonators
  - Structure and dynamics of sawteeth crashes in ASDEX Upgrade
  - Computer modeling of impurity clusters in steels.

The Technology Programme is carried at ICP UL - Institute of Chemical Physics, University of Latvia. The technology research and development under EFDA JET is focused on:

- Analysis of tritium distribution in plasma facing components
- Release of tritium from neutron-irradiated pebbles
- Radiolysis of plasma synthesized lithium orthosilicate nanopowders.

Several Staff Mobility actions took place in 2010: to IPP Garching, FZK Karlsruhe, UKAEA Culham, ISTTOK Lisbon, Meriland University.

2. FUSION PROGRAMME ORGANISTION

2.1 Programme Objectives

The Latvian Fusion Programme, under the Association EURATOM-University of Latvia, is fully integrated into the European Programme, which has set the long-term aim of the joint creation of prototype reactors for power stations to meet the needs of society: operational safety, environmental compatibility and economic viability. The objectives of the Latvian programme are: (i) to carry out high-level scientific and technological research in the field of nuclear fusion, (ii) to make a valuable and visible contribution to the European Fusion Programme and to the international ITER Project in our focus areas. This can be achieved by close collaboration with other Associations.

2.2 Association EURATOM-University of Latvia (AEUL)

The Latvian contribution to the European fusion programme began in 2000 in the form of cost-sharing actions (fixed contribution contracts with EURATOM). The Association was established on 19 December 2001 incorporating the existing cost-sharing actions into its work plan.

2.3 Fusion Research Units

The Latvian Research Unit of the Association EURATOM-University of Latvia consists of three Institutes of University of Latvia.

1. IP UL – Institute of Physics, University of Latvia
   32 Miera St., Salaspils LV-2169, Latvia.
   Phone +371 6 7944700, Fax. +371 6 7901214
2. ISSP UL – Institute of Solid State Physics, University of Latvia
   8 Kengaraga St., Riga LV-1063, Latvia.
   Phone +371 6 7187810, Fax. +371 6 7132778
3. ICP UL - Institute of Chemical Physics, University of Latvia
   4 Kronvalda Blvd., Riga LV-1010, Latvia.
   Phone +371 6 7033884, Fax. +371 6 7033884

2.4 Association Steering Committee

The research activities of the Latvian Association EURATOM-University of Latvia are directed by the Steering Committee, which comprises the following members in 2008:

Mr. Vito Marchese Scientific Oficer RTD – 14

Mr. Rugerio Gianella Scientific Oficer RTD – 14

Mr. Marc Pipeleers, Administration and finance, Unit J5, DG Research

Mrs. Irina Arhipova, Ministry of Education and Science

Mr. Ivars Lacis, University of Latvia

Mr. Andrejs Silins, Latvian Academy of Sciences

The Steering Committee had one meeting in 2010. This meeting was organised as video Conference on July 2, 2010 with remote participation of EU Commission representatives.

2.5 The Latvian Members in the EU Fusion Committees

Consultative Committee for the EURATOM Specific Research and Training Programme in the Field of Nuclear Energy-Fusion (CCE-FU)

Mr. Andris Sternberg, ISSP UL

EFDA Steering Committee

Mr. Andris Sternberg, ISSP UL

Governing Board for the Joint European Undertaking for ITER and the Development of Fusion Energy, "Fusion for Energy" (F4E GB)

Mrs. Maija Bundule, Latvian Academy of Sciences

Mr. Andris Sternberg, ISSP UL

EFDA Public Information Group(recently – Public Information Network – PIN)

Mr. Maris Kundzins, ISSP UL

2.6 Public Information

Conferences

Results of fusion research were presented at:

- The annual scientific conference of University of Latvia.
- The 26th and 27th Scientific Conferences of Institute of Solid State Physics, University of Latvia.
- International Conferences "Functional Materials and Nanotechnologies" (FM&NT-2010, FM&NT-2011) Riga, Institute of Solid State Physics, University of Latvia
- 3rd Progress Meeting on the GOT "EUROBREED" , Riga, 18-19 May, 2010.

Educational activities

Excursions at ISSP UL from schools were organized two to three times a month for PhD students from Latvian universities. Booklets about ISSP UL and EFDA were distributed.

Television, press

Presentation in the television broadcasts TV1, TV7, TV24 and interviews in the newspapers "Neatkarīgā rīta avīze" and "Latvijas avīze".

Presentations in Radio – popular science broadcast.

Popularization of science

Presentation in the TV programme "Science in Latvia",

Presentation in the programme "Researchers Night in Latvia" on 26th of September, 2010.

2.7 Funding and Research Volume 2010

In 2010 the expenditure of the Association EURATOM-University of Latvia was:

Item	Expenditure (EUR)
General Support (20% EU contribution)	
Physics	**363827**
TOTAL	**363827**
GOT EOROBREED	**2528**
HYDOBE	**9228**
Priority Actions (Additional 20% EU contribution)	**6000**
Missions and Secondments under the Agreement on Staff Mobility (100% EU contribution)	**14483**

3. PHYSICS PROGRAMME – FUSION PHYSICS

3.1. Developing and delivering of Ga installations for tests on ISTTOK and FTU

Principal investigator: E.Platacis.
Staff members:OLielausis,J.Freibergs, A.Klukins,J.Peinbergs, D.Peinbergs, K.Kravalis

3.1.1 Gallium jet power extraction capability.

Heat absorption and removal by heavy liquid metal free surface flows remains as one of the alternative concepts for the power exhaust in future fusion reactors. Definite expertise in solution of corresponding problems was gained during experiments with Ga jets on the small size Tokamak ISTTOK {R=0.46m; r=0.085m; B_t=0.45T; $T_e(0)$=150eV; $n_e(0)$=5x10^{18}m^{-3}; I_p≈6kA; V_p≈3V}{1;2;3]. The gallium jet was brought in contact with the plasma inside the discharge camber. It was stated that under such conditions ISTTOK can be successfully operated without degradation of the discharge, without a significant plasma contamination by the liquid metal. Definite induced by plasma modification of jets trajectory has been fixed, discussion on the reasons started. Finally, first conclusions about the jets power extraction capability were drawn. Let us concentrate exactly on this latest result described in our collaborative 2010 presentation [3]. The schematic cross-section of ISTTOK's vacuum chamber and of the implemented setup in the vicinity of the plasma-jet interaction region is presented in Fig.3.1.1.

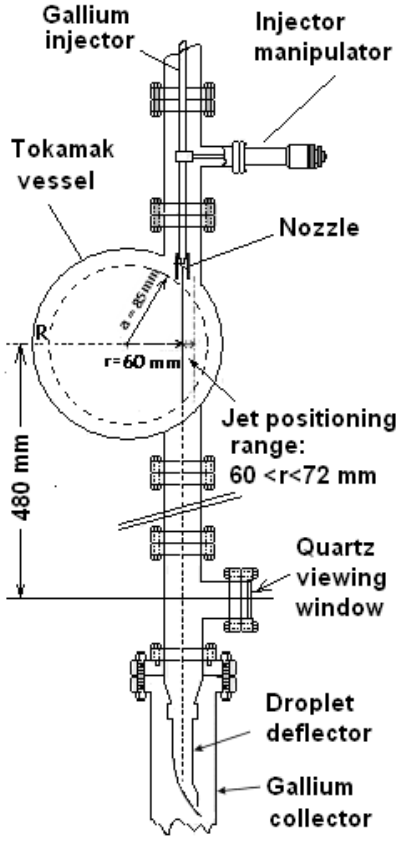

Fig.3.1.1. Cross-section of the discharge chamber of ISTTOK.

After passing the plasma through a placed below for approx. 0.5 m viewing window the corresponding increase of the jets surface temperature was measured using absolutely calibrated multi-channel IR sensors. At velocities under consideration (2.5m/s) during the 30 ms long discharge an approx. 6 cm long (diameter d = 0.23cm) segment of the jet becomes exposed to the plasma. The acting LM volume can be estimated at 0.25 cm^3. The temperature of this volume jumps for 103^0 C, it is the base to say that 2.4 kW have been extracted by the jet. The volumetric load is high indeed – 10 kW/cm^3. Some specific surface loads can also be deduced. Considering the load as frontal – 2.4 kW / (0.23x6) cm^2 = 1.9 kW/cm^2. Considering the load as distributed over the full surface of the jet – 2.4 kW / 4.3 cm^2= 0.6 kW/cm^2. Let us take something in the middle, say, 1 kW/cm^2 = 10 MW/m^2. Such a load is already fully divertor relevant. The high spatial stability of the jets body should be underlined. During the 30 ms long discharge the contour of the jet inside the plasma

was fixed on video. A practically stagnant picture could be seen, in spite of exposure of the jet to complex perturbations acting for the short 30 ms. In the same time after passing the plasma the jets trajectory along its full length becomes remarkably modified. The pictures inside the plasma are representing the situation directly (for approx.12cm) after the nozzle. In the region of the viewing window a definite deflection of the jet was fixed. The window is placed at a distance 496 mm below the equatorial plane. To produce the measured 10mm shift during the pulse duration (30ms) an average force of 4 mN should be applied to the acting element of the jet.

The demonstration of the fact that after touching the plasma the jets trajectory becomes modified should be considered as a next essential result of the Lisbon-Riga collaboration. In [1] a number of potential reasons for the jets replacement have been mentioned: mechanical stress in the injector due to chamber compression; MHD forces due to the presence of 3D magnetic field gradients; plasma kinetic pressure; induction of currents of in the full jet or in the segment of the jet immersed in plasma. Let us concentrate exactly on this latest rudimentary mechanism. The full liquid gallium loop installed on ISTTOK has been carefully designed to avoid large scale currents by using electrical isolators in specific positions along the circuit. However, as the prime circuit breaking mechanism the break-up of jets in droplets should be considered.

3.1.2 Break-up of liquid metal jets.

If the jet remains included in a closed electrical circuit directly induced jxB forces could lay behind after a great number of different instabilities. To disconnect the circuit the well known Rayleigh instability was used predicting that after a definite length each jet breaks up in droplets.

b) a)

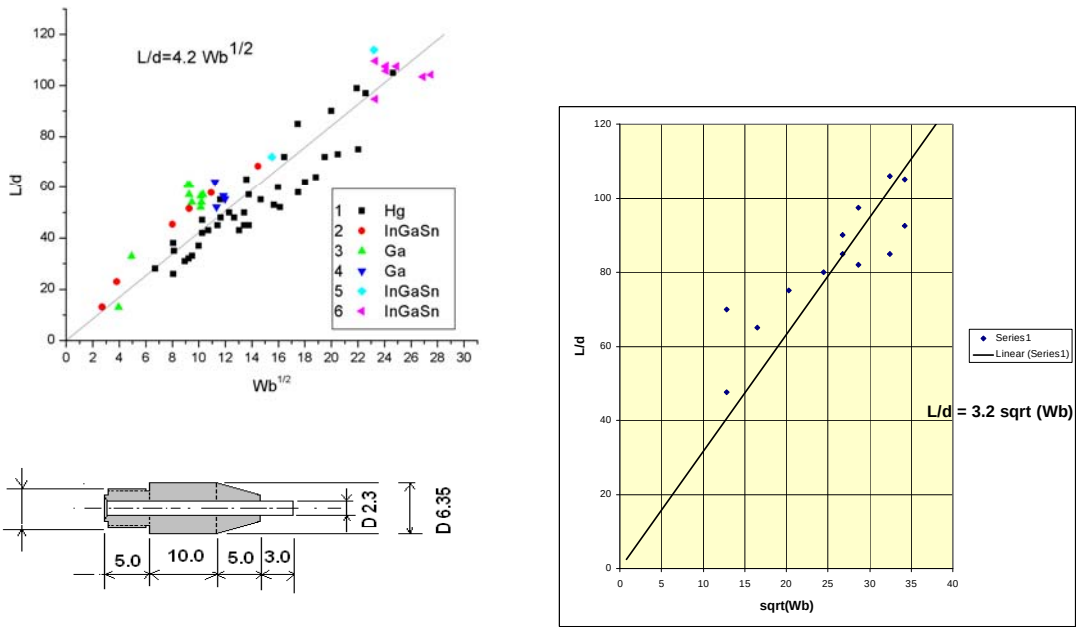

Fig.3.1.2. Determination of the break-up length for heavy liquid metal jets.

For the break-up of liquid metal jets results are presented in Fig.3.1.2a. With an acceptable accuracy the relative length of the continuous part of the jet can be described by a dependence on the Weber number: $L/d = 4.2\ We^{1/2}$, where "L" stays for the length of the continuous part of the jet and "d" for the diameter of the nozzle. The Weber number $We = \rho v^2 d / \sigma$ characterizes the ratio of the inertial forces to the surface tension forces and consists of the density ρ, velocity of the jet v, diameter of the nozzle d and surface tension σ. If a not very high accuracy is required such a linear dependence of L/d on $We^{1/2}$ can be used also in other branches of hydromechanics, in the so called quasi-turbulent regime. The physical parameters of the liquid as well as the conditions of the experiment can slightly influence the coefficient of proportionality or "stability". So, for water values 3.8-4.0 have been proposed. The represented in Fig.2a experiments were performed in the frame of our Lisbon-Riga collaboration. Simple cylindrical nozzles were used, the break-up point was determined bay photo/video techniques. The cross section of one of such nozzles has been shown on Fig.3.1.2b. It is worth mentioning that the presented expression stays valid also for a definite number of equally spaced nozzles (separated at least for 1.5-2 d). In such a context the points marked on Fig.3.1.2a by "5" should be considered as especially informative. These values have been taken from [4], a substantial article on MHD of liquid metal jets, describing a fully different set of experiments, specially shaped nozzles, etc. Fully independent are also results represented in Fig.3.1.2c. The corresponding values for treatment were found in [5]. Interesting are the parameters of this experiment - Hg jets issuing from a thin d=0.5mm nozzle with up to 10m/s velocities. And again, a linear dependence of L/D on $Wb^{1/2}$ can be deduced, with the coefficient of stability 3.2.

However, all the time the presence of strong magnetic fields should not to bee forgotten. Interesting tendencies in the development of free surface LM MHD flows were demonstrated already in [6]. In experiments with InGaSn in up to 4T fields great problems were detected at the generation of stable flows in flat open beds. On the other hand, at the generation of flat and round jets the influence of the field was clearly stabilizing. An expressed dampening of splashes at the targeting of jets against solid obstacles was also observed.

If the basic influence of the field remains stabilizing there were all grounds to expect that under conditions when a magnetic field is applied to the nozzle the break-up length should grow. Modeling experiments on mercury were performed [7] covering the range of nozzle diameters d = 1.0; 0.75; 0.5 and 0.25 mm and velocities up to 5 m/s. The nozzles were placed in a gap of an electromagnet with permendure field concentrators creating an up to 3.3T strong transverse magnetic field. It was stated that in a good enough approximation the relative increase of the break-up length L/L_0 can be described by a linear dependence on the relation Ha/Re, where L_0 stays for the discussed above break-up length without field, Ha and Re are representing the Hartman and Reynolds numbers. The length of the continuous part of the jet was measured by means of a displaceable electrical contact, an increase for up to 50% was stated.

In additional experiments InGaSn was used. Nozzles of d =1.5 mm and d =2.5 were placed in an up to 3.5T strong transverse field. An increase for up to 100% was reached. Again, in the first approximation the relation Ha/Re could be considered as the leading parameter, however, the dependence of L/L_0 on Ha/Re was more complex, already non linear. Efforts to bring these two results together are resulting in a fully empirical expression $L/L_0 = 1+0.75\ Ha^{1/3}/Re^{1/4}$. The accuracy of this expression is characterized by Fig.3.1.3. In spite of the rough approximation an opportunity appears

to form a definite understanding about the behavior of a jet under real reactor relevant conditions, about the intensity of the corresponding MHD interactions, etc. Let us consider the magnetic fields in the range 3-5 T, the velocities in the range 5-10 m/s and the diameters of the jets in the range of 5-7 mm. The corresponding values of the complex $Ha^{1/3}$ $Re^{-1/4}$ remain within the limits 0.4-0.7. According to Fig.3 it means that under conditions of real reactors a jet length increase for 30-50 % can be expected. And it is a remarkable number.

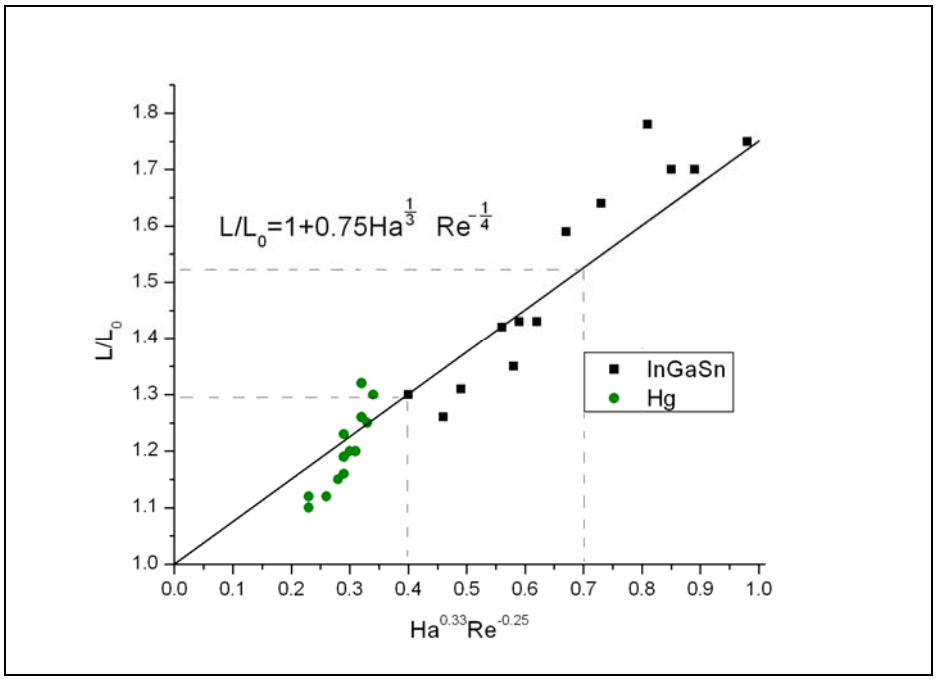

Fig.3.1,3 Increase of the break –up length if a magnetic field is applied to the nozzle.

3.1.3 Testing of active means for jets disintegration.

All the above considerations are leading to the conclusion that today we are able to predict the point of jets disintegration in a rather rough approximation. It is typical to estimates when hydro-mechanical instabilities have been included into consideration. In the above described experiments on ISTTOK the achieved accuracy in the determination on the location of the break-up point was fully acceptable since the construction of the vacuum chamber (Fig.3.1.1.) allowed for a free downward passage of the jet. However, in a general case not only a better accuracy is required .Typical is also the necessity for a controllable displacement of the point of jets disintegration. As an example the situation can be considered when it was necessary to transfer with the experiments from ISTTOK to the mock-up of FTU. On FTU the inlet of the hydraulic system becomes placed in a horizontal port and the outlet in a downward directed vertical port. The free flaying Ga jet must join these ports, touching upon plasma in the frame of SOL (Fig.3.1.4a).
Fig.3.1.4 corresponds to a version when exactly before the nozzle the jet is mechanically excited/perturbed in the range of frequencies $1\text{-}1*10^4$. The perturbations are introduced by means of a vibrating membrane (Fig.3.1.4b). On Fig.3.1.4c a photo is presented where the relative position of the vibrator with regard to the borders of the SOL can be seen. It was clear that because of the low introduced power not essential changes in the jets behavior should be expected. The installation was aimed mainly at a smart “adaptation” of the jets break-up point to the borders of the SOL

clearly marked in the mock-up. Fig.3.1.4d shows a situation when the break-up point is located already somewhat inside the SOL. Fig.3.1.4e demonstrates how the break-up point can be transferred directly to the outer border of the SOL.
Another version illustrates Fig.3.1.5 when the jet is partly stopped by an obstacle in the form of a flat plate. The geometry of the stopping installation is shown in Fig.3.1.5a. The location of the stopper with regard to the contour of the SOL inside the mock-up can be seen in Fig.3.1.5b.

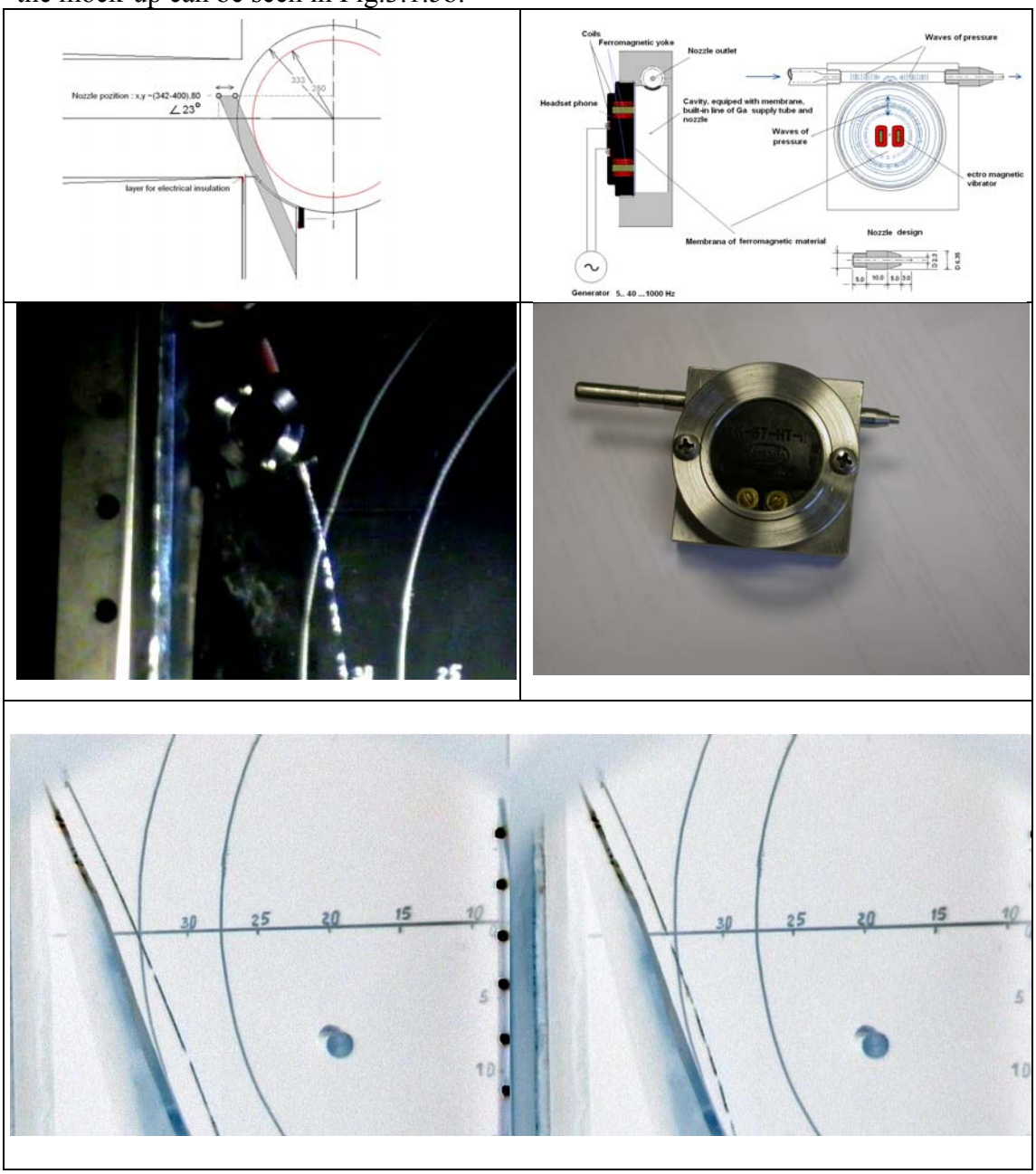

Fig.3.1.4. Shifting of the break-up point by slight mechanical perturbation of the jet.

To start feeling the influence of MHD interaction the jet was targeted against a thin Cu plate. The Cu layer was glued on the surface on a permanent magnet generating in the region of the flowing InGaSn an orthogonal magnetic field with the intensity of the order of 0.6 T. It means, in such a way a situation for the generation of the classical Hartman effects was ensured. For comparison, in another set of experiments

the Cu plate was glued on the surface of a non-magnetic body of the same shape. Crucial for these experiments is the role of the surface tension forces. After contacting a properly wetted Cu surface the round d=2.5mm jet becomes spread and flattened practically over the full 3 cm width of the breaking plate, both in the case with the magnet (Fig.3.1.5c) as well in the case without the magnet (Fig.3.1.5d). In Fig.3.1.5e and Fig.3.1.5f situations are presented when the jet is touching upon a Cu plate preliminary not wetted. The surface becomes wetted gradually by the jet itself. The phenomenon of spreading remains present, however, in a less expressed way. On the background of the direct and strong influence of the surface tension it was difficult to fix more ore less exactly the influence of the MHD forces. However, the work is in a very initial stage. To broaden the applicability of the results it is foreseen to define the dependences of the characteristic parameters on the Stuart and Weber numbers, it means, the dependences on the relation of the inertial forces to the electromagnetic and to the surface tension forces

a)

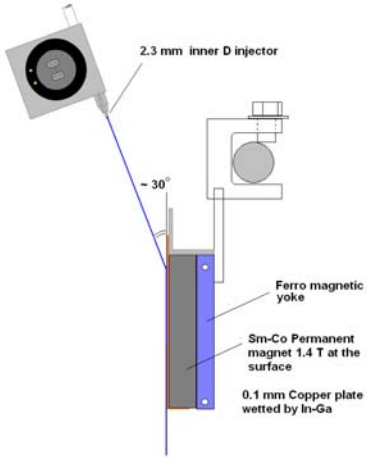

b)

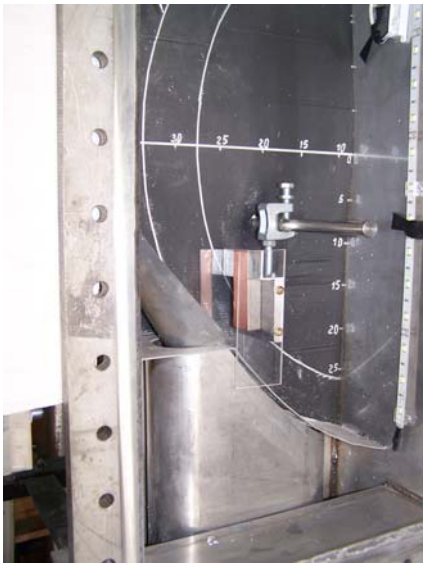

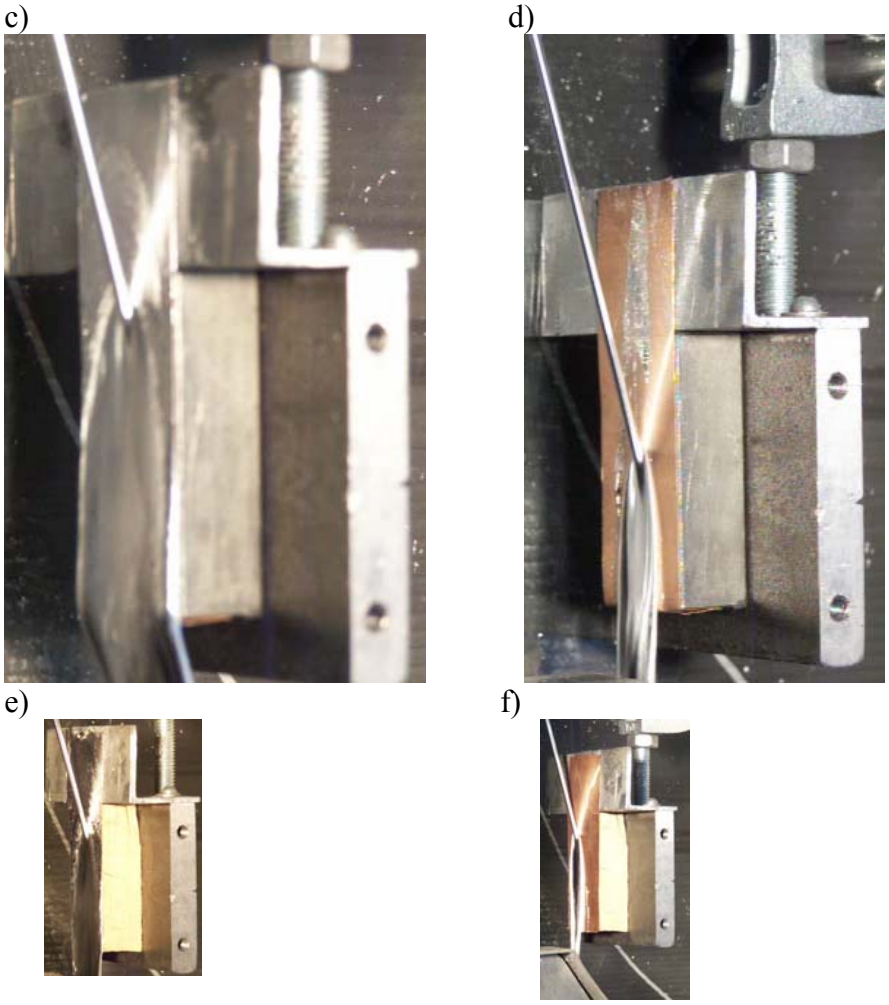

Fig.3.1.5. Breaking of a round jet after targeting against a flat obstacle.

The introduction in the practice of experiments active means for the control of the break-up process opens new opportunities at the application of jet-type liquid metal flows. However, crucial remains the result that heavy LM jets are able to withstand surprisingly high power loads after touching upon plasma.

References:

[1] Gomes R.B.,Fernandes H., Silva C., Sarakovskis A., Pereira T., Figueiredo J., Carvalho B., Soares A., Varandas C., Lielausis O., Klykin A., Platacis E., Tale I.: Interaction of liquid gallium jet with the tokamak ISTTOK edge plasma. Fusion Eng. & Des., 83(2008)102-111

[2] Gomes R.B.,Fernandes H., Silva C., Sarakovskis A., Pereira T., Figueiredo J., Carvalho B., Soares A., Duarte P., Varandas C., Lielausis O., Klykin A., Platacis E., Tale I., Alekseyev A.: Liquid gallium jet-plasma interaction studies in ISTTOK tokamak. Journ.of Nuclear Materials 390-391(2009)938-94

[3] Gomes R.B., Silva C., Fernandes H., Duarte P., Lielausis O., Klykin A., Platacis E. Dynamic behavior of a Liquid Gallium Jet under the influence of the Tokamak

ISTTOK Plasmas; 19 Internat. Conf. on Plasma Surface Interaction., P2-83, May 24-28 (2010) Sam Diego, USA.
[4] Ying A.Y., Abdou M.A., Morley N., Sketchley T., Wooley R., Burris J., Kaita R.,Fogarty P., Hung.H.,Lao X.,Narula M., Smoletsev, Ulrikson M.: Exploratory studies of flowing liquid metal divertor options for fusion relevant magnetic fields in the MTOR facility. Fusion Eng. & Des., 72 (2004) 35- 62
[5] Ansley W.E., Merryman S.A., Rose M .Characteristics of Liquid Mercury Jets and the Potential Application as an Opening Switch. Proc.Plasma Conf.,1,27 (1993)
[6] Bucenieks I., Lielausis O., Platacis, E.,Shishko A.: An experimental study of liquid metal film and jet flows in a strong magnetic field. Magnetohydrodynamics, v.30 n.2 (1994)179-187
[7] Bucenieks I., Lielausis O., Gerbeth G., Falk F.: Stabilization of thin liquid metal jets by magnetic field. 14th Intern. Riga Conf. on Magnetohydrodynamics, Jurmala,Latvia, 24-26 Aug. 1995, Book of Abstracts, p.14

3.2. Spectroscopy of Ga multijet vapours concentration and dynamics in tokamak plasma

Principal investigator: Dr. I. Tale

3.2.1 Background

The liquid Ga metal limiter experiment will be provided in collaboration between three Associations: ENEA Frascati, Italy, IST Lisbon, Portugal and AEUL, Riga, Latvia.

The project continues investigations arising from experimental results and problems with the single jet liquid metal limiter at tokamak IST, Portugal.

The goals for development of the Ga vapour spectroscopy at tokamak ENEA Frascati have been elaborated taking in account of the following results of experiments performed at IST ISTTOK.

- The presence of the jet in the chamber generates a pronounced increase in the emission of Ga vapour spectral lines. Evaporated Ga penetrates in the plasma and close to the jet surface is rapid ionized to higher ionization stages. (Ga, Ga^{+} and Ga^{2+} ionization potentials are respectively: 6.0, 20.5 and 30.7 eV).
- Penetration profiles of Ga and Ga ions in the plasma polodial plane are distinctive.
- Attempts to acquire spectra from a viewing located at $\varphi = \varphi_{jet} + 135°$ have proven themselves to be unfruitful since the intensity of gallium (either neutral or ionized) lines were lower than the sensor detection limit. Consequently the influence of the liquid metal jet on the plasma appears to be only a local perturbation since it is only observable at the jet position without any strong signals of plasma performance deterioration.
- Evaluation of the kinetics of Ga vapour concentration due to interaction with plasma shot serves important information for the Ga vapour creation and decay process.

According to the final plan the Ga multijet experiments at tokamak IST during 2010 will not performed. Task will be focused to development of the multijet liquid Ga experiments at ENEA, Frascati.

3.2.2. Goals

Development of the impurity spectroscopy in tokamak plasma at ENEA, Frascati:

- To design on of the optical system for acquiring the plasma emission in vertical and horizontal directions in the polodial plane of tokamak.
- To design of the time – resolved spectroscopy of plasma emission spectra in millisecond –second range.
- To design of the spectroscopy and the spectra acquisition systems.

Design of the equipment for Ga- multijet vapour spectroscopy at ENEA, Frascati.

3.2.3. Results

3.2.3.1. Concept of Ga vapour spectroscopy at ENEA, Frascati.

Following the analysis of experience of the Ga-vapour spectroscopy at experiments at IST, Portugal the preferred direction for investigation of the Ga vapour distribution is the polodial plane of tokamak. Taking into account that the liquid Ga jet will be injected in the underneath part of vessel the information about Ga vapour distribution is necessary to have both in the radial and in the vertical directions in polodial plane.
The full observable length of openings in radial and vertical direction is 400 mm, distance from vessel centre to objective about 800 mm. It is not realistic to perform the measurements using single object lens. Thus several object lenses are necessary to apply for measurements.
We assume that to obtain information about the distribution of Ga vapour concentration measurements in both directions shall be made at 10 to15 positions. The diameter of the plasma area to collect the emission intensity by focusing the object lens to the central plane of tokamak vessel shall be 20 – 40 mm.
Fiber optics design restricts the available image diameter of observed plasma emission area. The smallest circle diameter can be build by 7 fibers: one in centre surrounded by six ones.
Assuming that measurements of Ga emission spectra will be performed simultaneous in 20 positions (10 in radial, 10 in vertical dimensions) the total number of fibers reach 140. Taking into account that the diameter of smallest single fiber is 130 um, the maximal number of fiber available for illumination of the entry slit of spectrograph (6.7 mm) does not exceed 64 fibers.
Conclusion shall be drawn that the maximal number of simultaneous measured plasma emission spectra shall not exceed four positions for each - the radial and the vertical directions.
Full distribution of the Ga- vapour concentration can be collected performing information obtained in three successive plasma shots.

3.2.3.2. Setup of the equipment for Ga-vapour spectroscopy .

The setup of Ga-vapour spectroscopy involves the *in situ* optical system for collection of the plasma emission in polodial plane of tokamak and *remote* system for spectroscopy of plasma emission, spectral data acquisition, and time resolved control of equipment.
Both the vertical port and the horizontal port are equipped by four object lens systems. Images of the plasma emission in the centre plane of vessel are focused on the inputs individual ferrules of the fibre bundle. At the output end of fibre bundle the fibres are arranged in single line. Seven fibres corresponding of each eight input ferule are separated by gaps corresponding two unexposed horizontal pixel lines of ICCD camera.

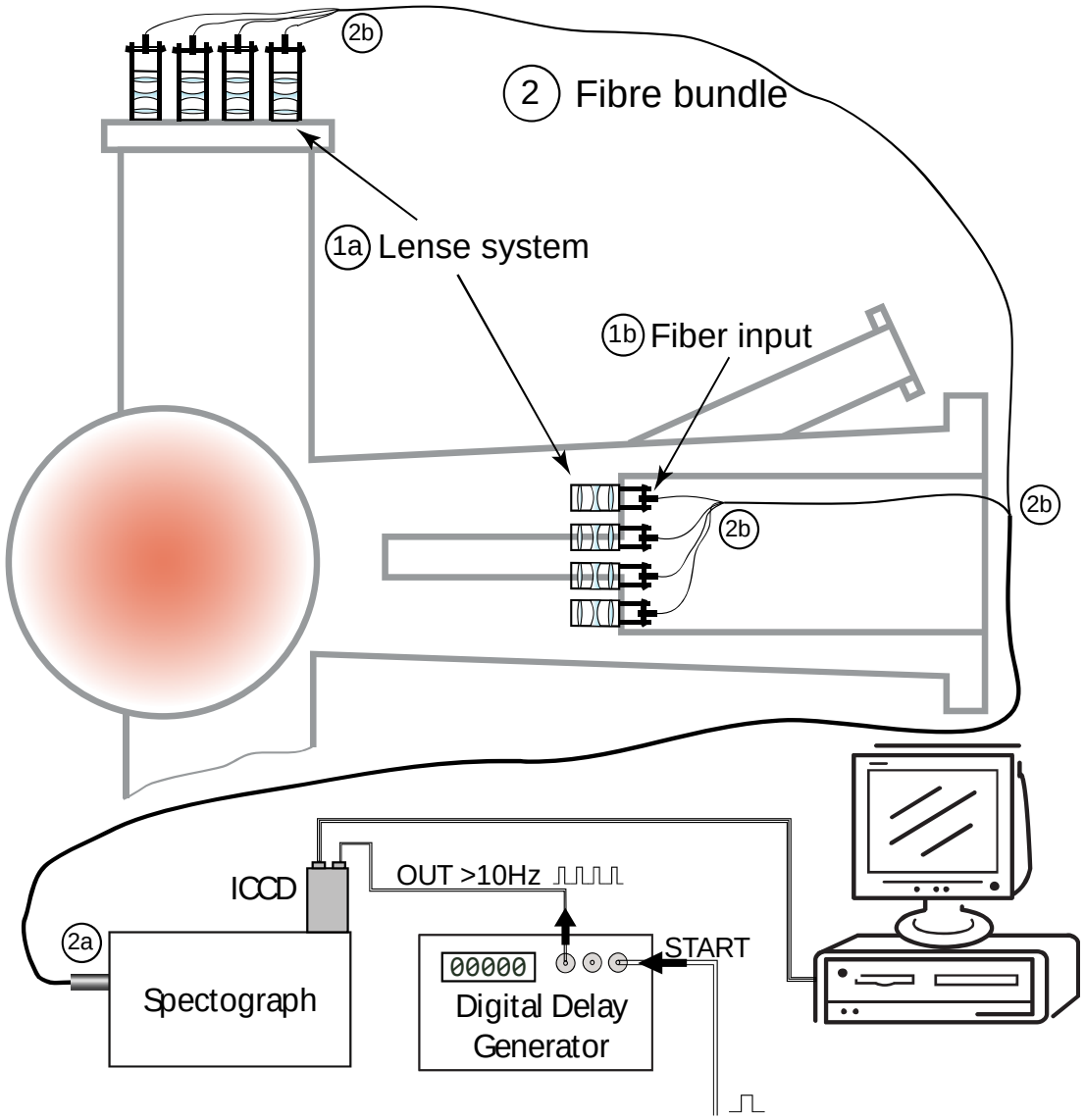

Figure 3.2.3.1. The setup of equipment for time-resolved spectroscopy of Ga vapour emission in the liquid Ga experiment at tokamak ENEA, Frascati.

The fibre bundle's output ferule is arranged to the input focal plane of spectrograph. Emission spectrum is detected by ICCD (Intensified CCD) camera. The ICCD camera used ensures reach the exposition – data acquisition time less than 100 ms. Spectral data of plasma emission are accumulated by PC. Time resolved spectra measurements, positioning of the entry ferules of fibre optics for multiple emission spectra measurements at different plasma positions are controlled by PC. Separate delay generator will be installed for tome resolved spectra accumulation during the whole plasma shot.

Figure 3.2.3.2 represents the optical system for collection of the plasma emission in tokamak polodial plane on the spectrograph entry slit.

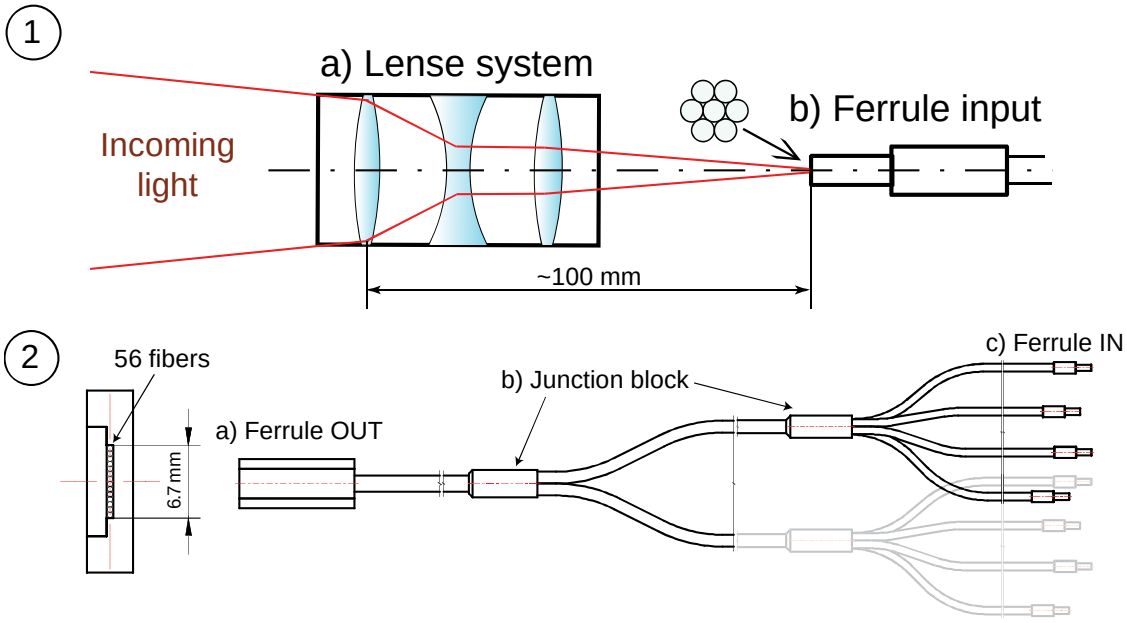

Figure 3.2.3.2. Design of the object lens and fiber bundle.

Object lens is represented by typical three lens combination allowing adjust both the input aperture and the output aperture. The fiber bundle is assembled by the fiber sub bundles. The optical parameters of the fiber bundle conform to the requirements of spectrograph ANDOR Shamrock Czerny-Turner series spectrograph at the output and the diameter of plasma image on the input.

3.2.3.4. Design of the optical ports assigned for Ga-vapour spectroscopy.

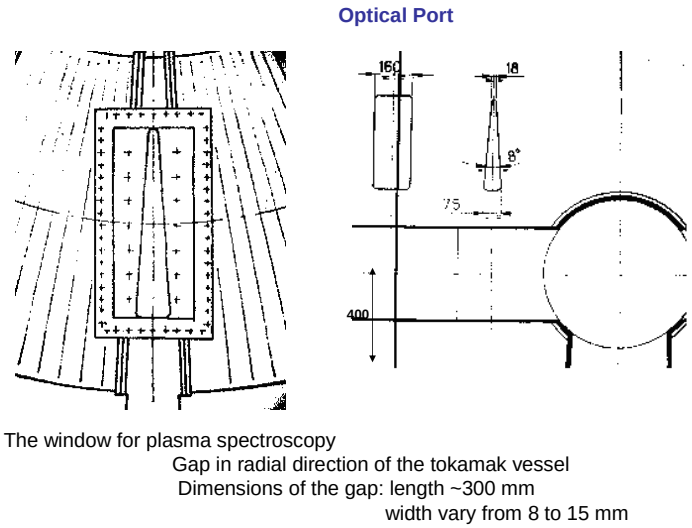

Figure 3.2.3.3. The vertical optical port. The rectangle viewing area of the horizontal optical port 160 x 400 nm. The gap in the radial direction has dimensions ~300 mm in the length and varying width from 8 to 15 mm.

Four object lenses will be mounted on the holder plate. The fiber in put ferules for individual adjustment will be mounted on xy translation stages. The stages will be fastened on the linear translation stage controlled by the step motor for remote switching of the plasma observation position.
The horizontal port will by used both for the equipment for transporting of liquid Ga and for the collection of the plasma emission. The rectangle opening dimensions are 400 x 160 mm. The available gap for optical measurement in torodial direction is 400 x 15 mm. Design of the horizontal port is represented in Figure 3.2.3.4.

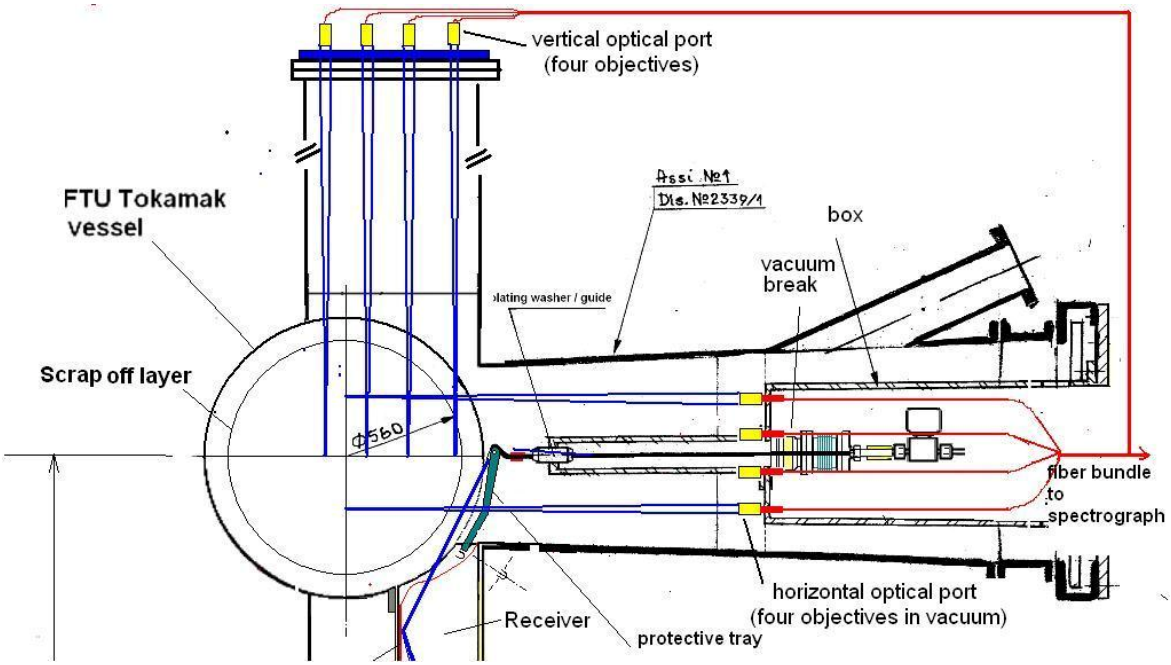

Figure 3.2.3.4. The equipment for supply of the liquid Ga in the vessel and mount of the objet lens system on the box.

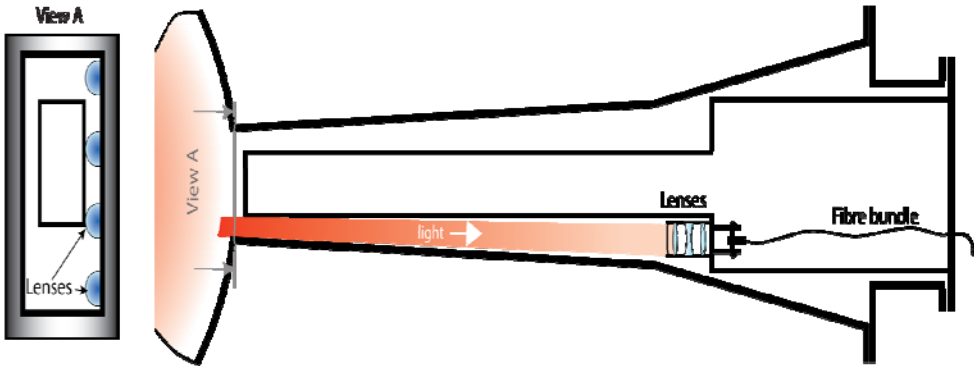

Figure 3.2.3.5.The radial view of object lens positions (left); the top view top view object lenses positions.

The equipment foe supply of liquid Ga jet is positioned in centre of the rectangle gap. Two vertical gaps can be used for the plasma viewing in the left or right side of the liquid Ga equipment. Dimensions of each gap are 15 x 400 mm.
Two design versions of object lens have been considered: object lens in vacuum – fiber bundle ferules in air, both the object lens and fiber bundle ferules in air. Design depends on the requirements of liquid Ga support system.

3.2.3.5 Time-resolved spectroscopy

To detect the Ga vapour emission spectra a high sensitivity ICCD camera will be used.
For time resolved spectroscopy important requirement for ICCD camera is the shortest time duration, necessary for data transfer of each spectrum frame during the plasma event. The iStar 720 ICCD camera is found the best available which includes an optional digital delay generator, actually built into the head.
This unique system is designed for low-light spectroscopy applications requiring fast gating.
The 1024 x 256 array has a 4:1 aspect ratio making it ideally suited to use with an imaging spectrograph such as the Andor Shamrock 303i.
A wide selection of photocathode options provides a range of solutions, whether you need a broad spectral response or optimization in a particular wavelength region
The unique remote control allows the user to operate the system up to a distance of 12m from the receiver.
Data transfer time for single spectrum do net exceeds 50 ms and 12 frames per second can be obtained.

Technical Specifications of iStar 720.

Active Area (mm)	18 x 6.7 (18mm tube)
Active Pixels	690 x 256 (18mm tube) or
Pixel Size (μm)	26
Read Noise (e-, typical)	8 @ 31kHz
Spectral Range (nm)	380 - 980

3.2.3.6. System for multiplication of the plasma emission measurement positions in poloidal plane.

To obtain information about the distribution of Ga vapour concentration it is reasonable to perform measurements at 10 to 15 positions both in the vertical and the horizontal directions in polodial plane.
Corresponding diameter of the plasma volume to collect the Ga emission intensity can be up to 40 mm.
The focused light diameter at the entry end of fibre bundle is determined by diameter of optical fibres. The smallest circle diameter can be build by 7 fibres: one in centre surrounded by six one.
Length of the fibre line at output end of bundle is restricted by length of the entry slit of spectrograph and ICCD camera (6.7 mm).
The diameter of smallest single fibre is 120 mm. The maximal number of fibres does not exceed 56. Measurements in eight positions (4 in radial and 4 in vertical directions) can be simultaneous provided.
For multiplication of viewing directions we have developed system having four objective lenses stationary fixed at vertical and horizontal ports of tokamak. Each four

entry ends of fibre bundle are fixed at corresponding linear stages. They are adjusted for receiving of plasma emission in equidistant positions in vessel. Common shift of fibre bundle entry ends using linear stage results in shift of viewing direction plasma in vessel. And will be performed by remote controlled step motors.
To increase number of positions the plasma observation direction two spectra evaluation scenarios will be available.

- Measurements of full sequence in four positions during the whole plasma shot event followed by shift of the observation position from shot to shot.
- Shift of observation position from spectrum frame to frame e.g. multiplication by two or three at respectively decreased number for each position.

3.2.4. Conclusions

Development on of the optical system for acquiring the plasma emission in both the vertical and the horizontal directions in the polodial plane of tokamak have been performed.

Development of the technique for time- resolved spectroscopy of plasma emission in up to 12 positions of the tokamak plasma is performed.

Simultaneous measurements of the evolution of plasma emission spectra during the whole plasma pulse in mutually perpendicular directions performed in multiple positions will *for the first time* serve additional information about the dynamics of both, the distribution of liquid metal vapour - other impurity concentration and the plasma temperature in the tokamak vessel polodial plane.

Equipment necessary for installation of liquid metal vapour spectroscopy at tokamak ENEA, Frascati has been optimized and completed.

3.3. Theory and code development

Principal investigator: Dr. V. Kuzovkov

3.3.1. On the theory of high-power gyrotrons with uptapered resonators

O. Dumbrajs (AEUL), G.S. Nusinovich (*Institute for Research in Electronics and Applied Physics, University of Maryland, USA)*

In high-power gyrotrons it is desirable to combine an optimal resonator length with the optimal value of the resonator quality factor. In resonators with the constant radius of the central part, the possibilities of this combination are limited because the quality factor of the resonator sharply increases with its length. Therefore, the attempts to increase the length for maximizing the efficiency leads to such increase of the quality factor which makes the optimal current too small. Resonators with slightly uptapered profiles offer more flexibility in this regard. In such resonators, one can separate optimization of the interaction length from optimization of the quality factor, because the quality factor determined by diffractive losses can be reduced by increasing the angle of uptapering. These issues were analyzed in collaboration with Maryland University, by studying a typical high-power 170GHz gyrotron which is currently under development in Europe for ITER (http://en.wikipedia.org/wiki/ITER). The effect of a slight uptapering of the resonator wall on the efficiency enhancement and the purity of the radiation spectrum in the process of the gyrotron start-up and power modulation are studied. Results show that optimal modification of the shape of a slightly uptapered resonator may result in increasing the gyrotron power from 1052 kW to1360 kW.

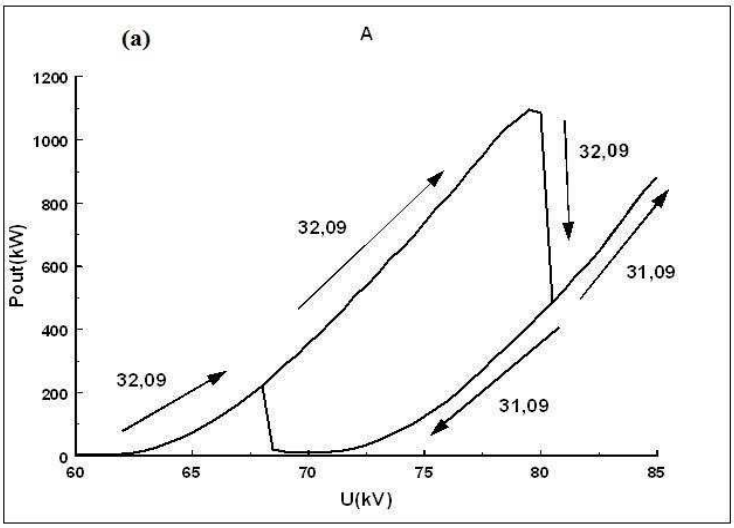

Fig.3.3.1. 1**.** Output power as a function of voltage in a gyrotron with the cavity. Calculations were carried out from 60 kV to 85 kV and from 85 kV to 60 kV. The parasitic $TE_{31,0}$ is excited at 80.5 kV. Due to the hysteresis, this mode survives when the voltage decreases until 64.5 kV where the operating $TE_{32,09}$ mode reappears. A clear hysteresis loop is observed.

3.3.2. Structure and dynamics of sawteeth crashes in ASDEX Upgrade

O. Dumbrajs (AEUL), V. Igochine, S. Günter, H. Zohm, K. Lackner, G. Pereverzev (*MPI für Plasmaphysik, Garching, Germany*), J. Boom, I. Classen (*FOM-Institute voor Plasmafysica Rijnhuizen, Nieuwegein, The Netherlands*)

The crash phase of the sawteeth in ASDEX Upgrade tokamak was investigated in detail by means of soft X-ray (SXR) and electron cyclotron emission (ECE) diagnostics. Analysis of pre-cursor and post-cursor (1,1) modes shows that the crash does not affect the position of the resonant surface q=1. Our experimental results suggest that sawtooth crash models should contain two ingredients to be consistent with experimental observations: (1) the (1,1) mode structure should survive the crash; (2) the flux changes should be small to preserve the position of the q=1 surface close to its original location. Detailed structure of the reconnection point was investigated with ECE imaging diagnostic. It is shown that reconnection starts locally. The expelled core is hot which is consistent with SXR tomography results. The observed results can be explained in the framework of a stochastic model.

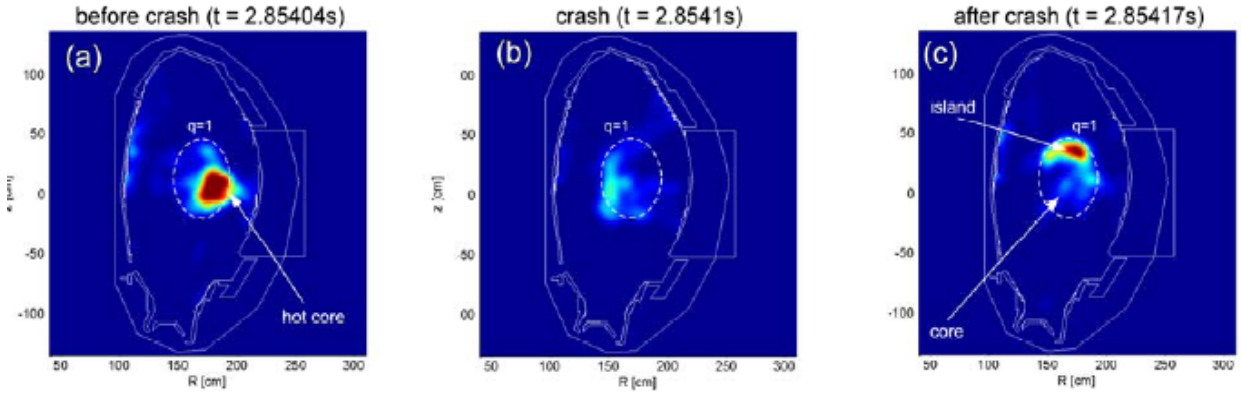

Fig. 3.3.2.1. Soft X-ray tomography of the sawtooth crash (t = 2.85s). Three different time frames are shown: (a) hot core rotates in clockwise direction before the crash; (b) crash phase; (c) hot island rotates in clockwise direction after the crash. q = 1 position is marked by the dashed line. (Each figure has its own color scheme to increase the contrast.)

It should be noted that electrons with different azimuthal coordinates of guiding centers exhibit different dynamics in the process of mode switching. This can be considered as a specific feature of the electron interaction with the fields of more than one mode. In the case of single-mode operation, electrons with different azimuthal coordinates of guiding centers exhibit the same behavior in the phase space. However, in the process of mode switching, where two modes are present, electron dynamics depends on the azimuthal coordinate of the guiding center. This can be explained by the fact that the phase difference of these modes is azimuthally dependent. This conclusion can be illustrated by the right figure in the second row in Fig. 3 showing electron distribution at the exit for t = 72.

Publications:

1. O. Dumbrajs, V. Igochine, A. Gude, M. Maraschek, H. Zohm, and ASDEX Upgrade Team, Temporal evolution of neoclassical tearing modes in the frequently interrupted regime. - *Phys. Plasmas*, 2010, 17, 042118 (p. 1-5).
2. V. Igochine, J. Boom, I. Classen, O. Dumbrajs, S. Günter, K. Lackner, G. Pereverzev, H. Zohm, and ASDEX Upgrade Team, Structure and dynamics of sawteeth crashes in ASDEX Upgrade. - *Phys. Plasmas*, 2010, 17, 122506 (p. 1-7).
3. O. Dumbrajs, V. Igochine, A. Gude, M. Maraschek, H. Zohm and ASDEX Upgrade Team, "Temporal evolution of neoclassical tearing modes in the frequently interrupted regtime". Abstracts of 26th ISSP Conference (Riga, Latvia, February, 2010): p. 55.

3.3.3. Computer modeling of impurity clusters in ODS steels

A. Gopejenko, Yu. Zhukovskii, E. Kotomin,
P.V. Vladimirov, A. Möslang (*Institut für Materialforschung I, Karlsruhe, Germany*)
V.A. Borodin (*Research Center Kurchatov Institute, Moscow, Russia*)

Reduced activation steels strengthened by Y_2O_3 precipitates (ODS) are promising structure materials for future fusion reactors. Both size and spatial distributions of oxides significantly affect mechanical properties and ODS radiation resistance. Development of ODS steels requires a deep understanding of the mechanism and kinetics of Y_2O_3 nanoparticle precipitation in the steel matrix. Therefore, it is necessary to perform a large-scale theoretical modeling of the Y_2O_3 formation. A series of first principles DFT plane-wave calculations were performed in *collaboration with Dr. A. Möslang and Dr. P.V. Vladimirov (Institut für Materialforschung I, Karlsruhe, Germany)* on different nanoclusters consisting of pair and triple solute atoms and containing: (*i*) the Y−Fe-vacancy pairs, (*ii*) the two Y atoms substituted for Fe lattice atoms and (*iii*) the O impurity atoms dissolved in *fcc*-Fe matrix. The latter is represented by a face-centered cubic γ-Fe single crystal. This structure is relevant because a phase transition $\alpha \rightarrow \gamma$ occurs in low Cr ferritic-martensitic steels at typically hot isostatic pressing temperatures. The results clearly demonstrate a certain attraction between the Y substitute and Fe vacancy or O impurity atom whereas no binding was found between the two Y substitute atoms.

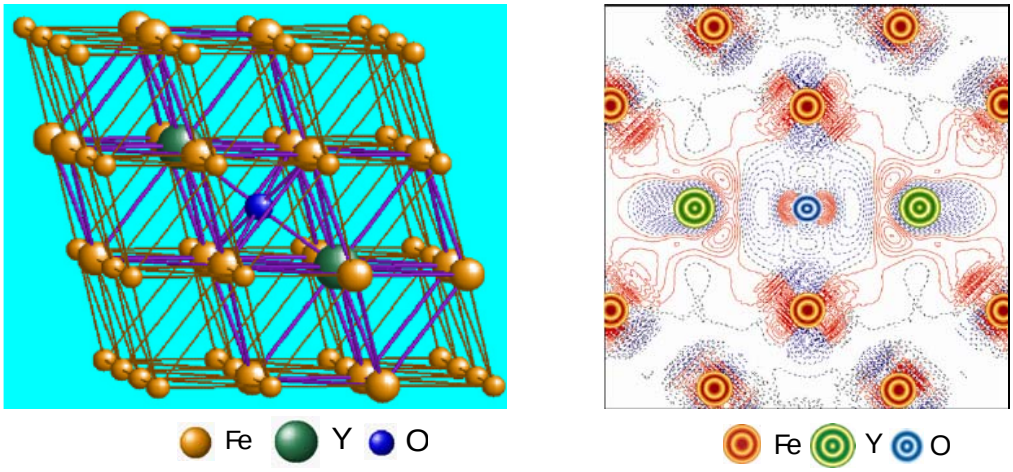

Figure 3.3.3.1. Alternative model of Y_2O nanocluster appeared in the γ-Fe lattice and re-distribution of the electronic density due to influence of this precipitate.

Calculations on different Y-O-Y cluster configurations in lattice (Fig. 3.3.3.1) show that not only a presence of oxygen atom favors a certain binding between the impurity atoms inside the γ-Fe lattice but also the increased concentration of Fe vacancies is required for the growth of the Y_2O_3 precipitates within the Fe matrix. To estimate energy barriers for migration of Y and O impurity atoms as well as Fe vacancies we have performed a series of test calculations using Nudge Elastic Band method.

Both interaction energies between solute and matrix atoms and barriers for diffusion of different solute atoms are extracted from these calculations for further atomistic simulations at the second step of theoretical study within the formalism of lattice kinetic Monte Carlo (LKMC).

Publications:

1. A. Gopejenko, Yu.F. Zhukovskii, P.V. Vladimirov, E.A. Kotomin, and A. Möslang, *Ab initio* simulation of yttrium oxide nanocluster formation on *fcc* Fe lattice. - *J. Nucl. Mater.*, 2010, 406, p. 345–350.

2. A. Gopejenko, Yu.F. Zhukovskii, P.V. Vladimirov, E.A. Kotomin and A. Möslang, "Y, O and Fe vacancy defect complex modeling in *fcc* Fe lattice". 26th ISSP Conference (Riga, Latvia, February, 2010), Abstracts: p. 30.

3. A. Gopejenko, Yu.F. Zhukovskii, P.V. Vladimirov, E.A. Kotomin, and A. Möslang, "*Ab initio* calculations of yttrium and vacancy point defects for ODS steels modeling". 7th International conference "Functional materials and nanotechnologies" FMNT-2010 (Riga, Latvia, March, 2010), Abstracts: p. 182.

4. A. Gopejenko, Yu.F. Zhukovskii, P.V. Vladimirov, E.A. Kotomin, and A. Möslang, "Simulation of yttrium oxide particle formation in iron in support of ODS steel development". 8th International Conference "Information Technologies and Management", IT&M'2010 (Riga, Latvia, April, 2010), Abstracts: p. 20-21.

5. A. Gopejenko, Yu.F. Zhukovskii, P.V. Vladimirov, E.A. Kotomin, and A. Möslang, „Pair and triple point defect complex modeling in *fcc* Fe lattice". Spring European Materials Research Society (E-MRS) Meeting (Strasbourg, France, June, 2010), Abstracts: NPVI-13.

4. EFDA FUSION TECHNOLOGY PROGRAMME

4.1. Tritium depth profiles of the carbon based jet tiles

Principal investigator: G.Kizane

4.1.1 Introduction

Carbon fiber composites (CFC) are a candidate material for divertor areas near the plasma strike points in future fusion devices. CFC tiles have been widely used for the first wall of the Join European Torus (JET) in order to investigate and estimate an applicability of the CFC for a future fusion machine. In ITER surface area of the CFC tiles will be 55 m^2 and at least 2 g of tritium per pulse will be accumulated in CFC tiles. Retention of tritium in plasma facing materials will limit ITER operation. Relatively a large fraction of the total tritium retained had migrated deep into the bulk of the tile. Tritium accumulation in the CFC tiles is a significant safety and waste handling issue. Tritium may cause an environmental hazard in emergency, problems with a level of wastes and it also is not desirable from the view point of economy the fuel as tritium will be incorporated and loosed.
Mechanisms of fuel retention and desorption is not completely clarified. The amount of the accumulated tritium depends of on the materials of a fusion device and of on the plasmas operation conditions. Under action of plasma large amounts of carbon are introduced into the plasma edge and then re-deposited at different locations of the chamber together with the hydrogen isotopes. The larger amount of tritium is co-deposited with carbon particles on a surface of materials. It is important to determine the tritium amount accumulated in the bulk of those tiles and to estimate the conditions that have an effect on that accumulation. Tritium retention in the deposited layers and in the bulk of the CFC is very much influenced by various factors. Structure and chemical composition are assumed to have an influence on tritium, energy of tritium ions, magnetic field and others.

The tasks JW10-FT-3.62 and JW9-FT-3.46 are related to the estimation of the tritium distribution in the carbon based tiles and are continuation of the EFDA JET Technology Tasks on the tritium in tokamaks.
Goals of the task are to determine depth profiles of tritium trapped in the bulk of CFC tiles, make comparison of tritium activities in the bulk and surface layers, estimate changes of structure of a tile, to investigate properties of the tritium trapped in CFC tiles. The samples for analysis of tritium were prepared by standard methods and determination of tritium in a separate sample was realized by full combustion or wet oxidation method and liquids scintillation method.

4.1.2 Experimental

Tritium distribution has been analyzed in the selected tile of the JET MkII Septum Replace Plate (SRP) divertor. The MkII Septum Replace Plate (SRP) divertor was used in 2001-2004 operation periods of JET. In the MkII-SRP divertor the septum structure of the MkII-GB divertor was replacing with a simple carbon fiber plate (Fig. 4.1.1.). Tile 14BWG4B was analyzed for realization the task. The tile is made of

Carbon Fibre Composite, Concept I manufactured by Dunlop Ltd. The tile is 2D woven fiber and is manufactured from fiber reinforced graphite by chemical vapor deposition with methane. During the operation period the divertor temperature was about 200°C, the backside was cooled and bulk temperature of the tile between pulses was about 100 °C. Tritium in vacuum chamber was introduced by gas puffing, neutral beam injection. In the year 2003 Trace Tritium Experiment had been performed with an introduction of 380 mg tritium into the vacuum chamber. There tritium was as a thermalized T+, fast tritium with energy about 100 keV and with energy up to 1 MeV as a result of D-D reactions. The integrated ion flux was in order 10^{27} ions.m^{-3}, neutron flux was $3.6 \cdot 10^{14}$ n·cm^{-2}. Estimated that 66 g of deuterium input retained in the vessel, what is approximately 4 % of total deuterium. The tritium accumulation dominates on the inner divertor shadowed areas.
Samples for analysis of tritium and structure were made by core-drilling method. Cylinders (ø 1mm) were cut from CFC tiles and sliced into separate disks of thickness 1 mm. In order to determine the tritium content in the separate carbon discs, the full combustion technique was used. Liquid scintillation method was used for measurements of tritium.

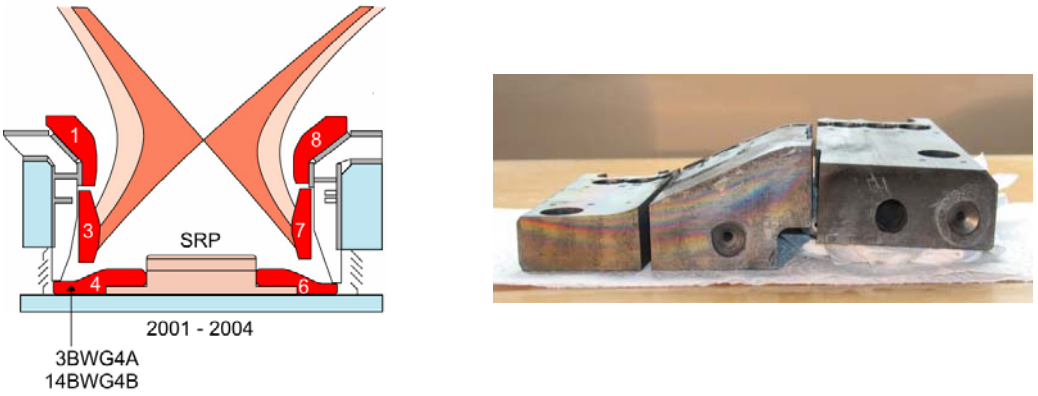

Fig.4.1.1. Scheme of the JET Mark-II-Gas-Box type divertor with a septum replacement plate (SRP) and photo of the divertor tile from the JET.

In the year 2010 analysis of tritium was continued for core-drilled cylinders of tile 14BWG4B Fig. 4.1.1. Core drilling positions of tile 14BWG4B for tritium analysis in a poloidal and toroidal direction are shown in Fig. 4.1.2.

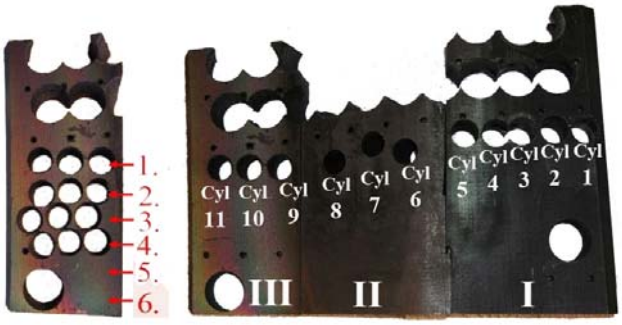

Fig. 4.1.2. Core drilling positions of tile 14BWG4B for tritium analysis in the poloidal and the toroidal directions.

4.1.3 Results

Carbon fiber composites are inhomogeneous materials, tritium migration and trapping in the fibre matrix, fiber core and sheath are considerable. Migration of tritium into the bulk of a tile is expected at high temperatures as is clearly demonstrated in the results from the sloping part where the tritium mass activity of the bulk was found to be about an order higher that in other parts of the tile.
Concentration of tritium in the surface layers and in the bulk is connected with the thickness of deposition layer, with energy of implanted tritium ions and with the energy of plasma deposited on a tile. Increase of the space between the sheath graphite planes facilitates the transport of tritium between the planes, while full destruction of fiber sheath leads to the increase of specific surface area and concentration of high energy trapping sites. The shadowed part of tile 4B is protected by a tile 3B.
Tritium activity in the slice 1 (A1) of Cylinder 2 up to Cylinder 10 of the Line 2 is not uniform, as previously determinate the sequence is the same, concentration of tritium at the septum replace plate is much more less than at the louvers side (Fig.4.1.3.).
Tritium depth profile also is uniform of the Cylinder 9 which is placed near to the louvers side for the lines 1up to the line 5. Amount of tritium is in the range of one order some kBg.g^{-1}(Fig.4.1.4.).

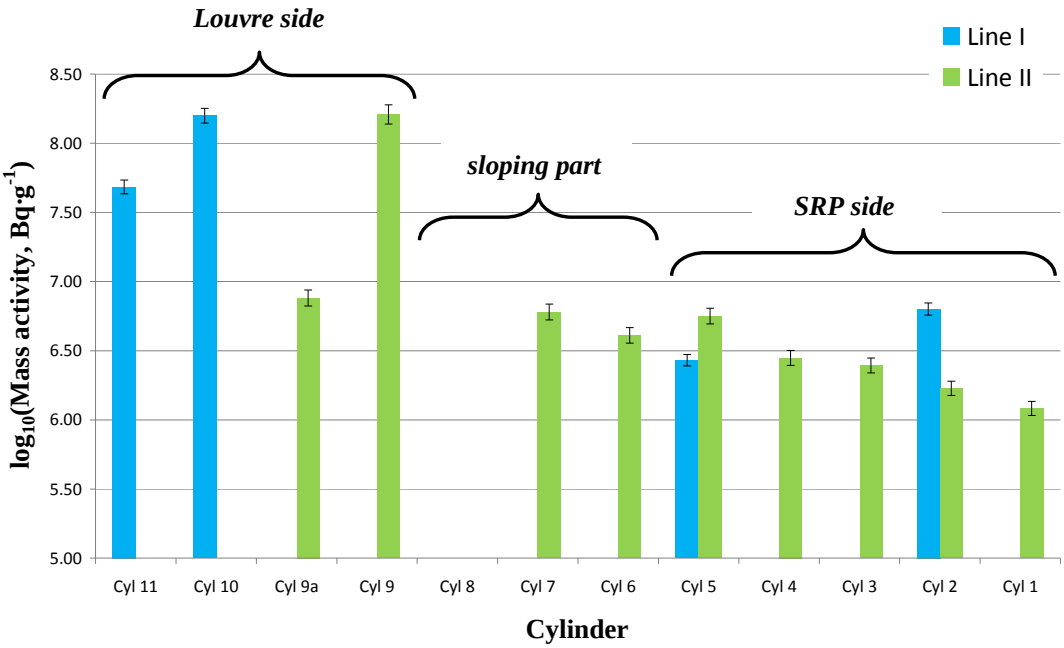

Fig. 4.1.3. Tritium activity in the first slice A1, lines 1 and 2

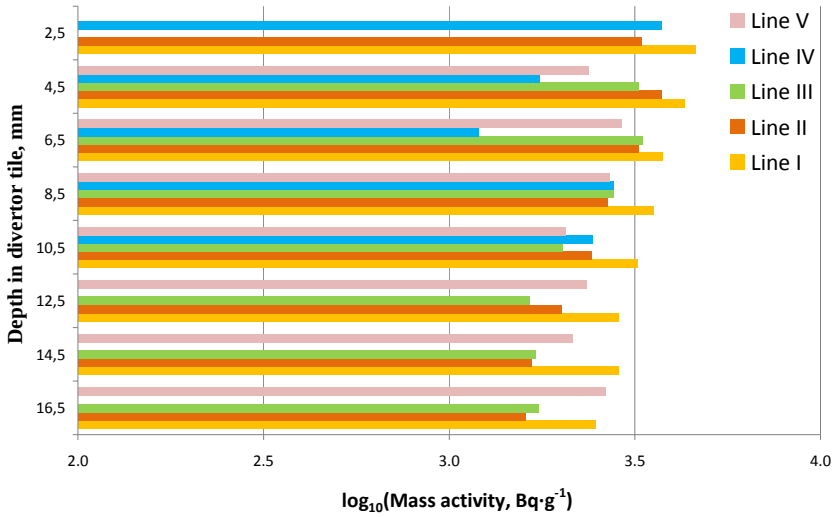

Fig.4.1.4.Tritium activity in bulk of Cylinder 9 at the louvers side, Lines I - V

Detailed analysis of the tritium distribution in the cylinders of the first line shows the analogous situation as described previously. The large part of tritium is concentrated in the first slices A1 (1 mm) for all cylinders. In the next slice the tritium amount sharply decreases and stayed less or more uniform in the middle of tile and then slightly increases. Migration of tritium into the bulk of a tile may be expected at high temperatures. The surface of the sloping part of the tile may reach even 1000^{o}C during plasma exposure.

Analysis of surface activity of tritium once more confirm the fact that main part of tritium is accumulated in a deposited. It can also be seen in the full profiles of cylinder line I (Fig. 4.1.5.) and line II (Fig. 4.1.6.). Surface- type image of cylinder line I is shown in Fig. 4.1.7.

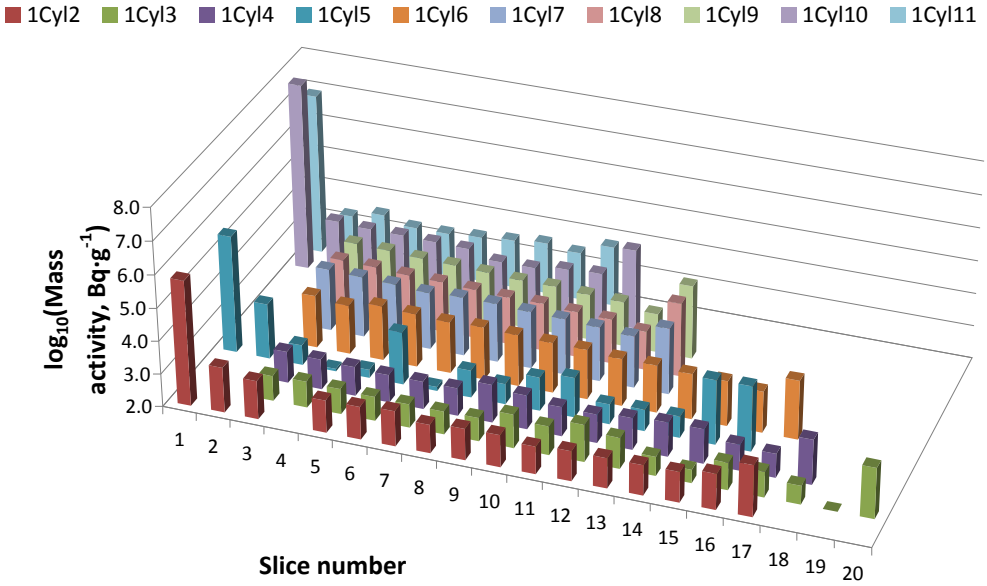

Fig.4.1.5. Distribution of tritium in the cylinders from 2 to 11 of the 1st line

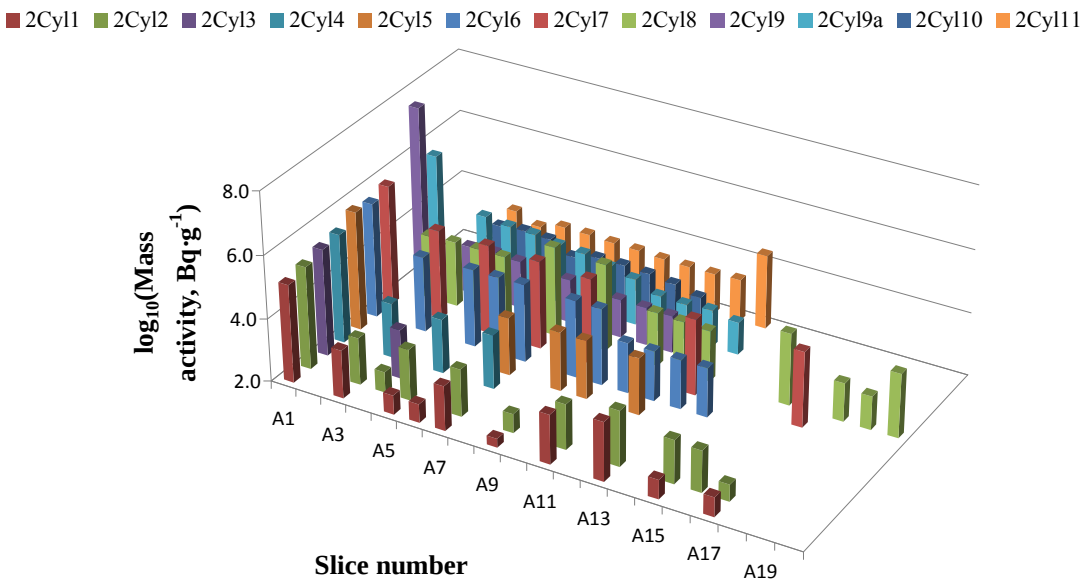

Fig.4.1.6. Distribution of tritium in the cylinders from 1 to 11 of the 2nd line

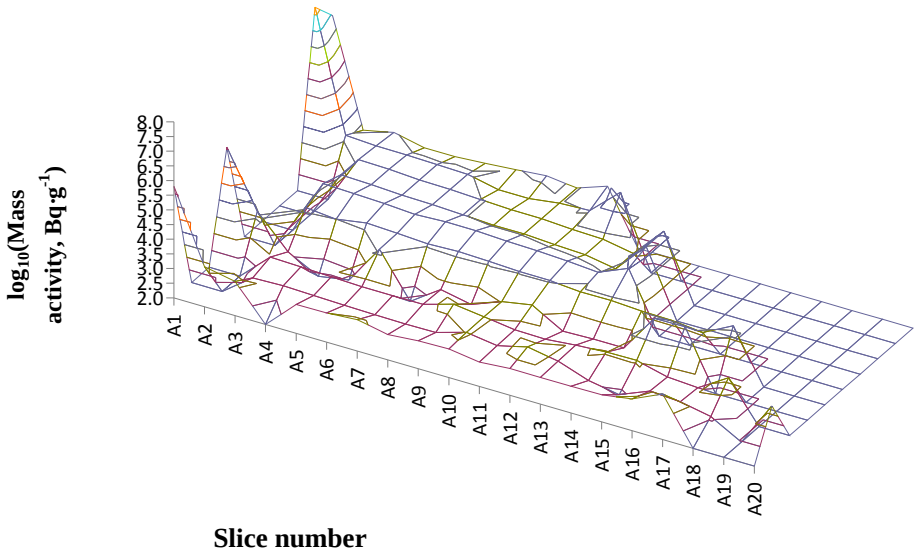

Fig.4.1.7. Surface profile of tritium in the cylinders from 2 to 11 of the 1st line

Desorption spectra of tritium from plasma exposed surface slices under action of temperature for all three investigated samples are different. The thermo-desorption spectra has additional shoulders for the slices of the cylinders 1 and 5. Common feature for all is that tritium release starts at ≤ 200 °C, the release rate reaches a maximum at < 680 °C and decreases rapidly at temperatures above 950 °C.

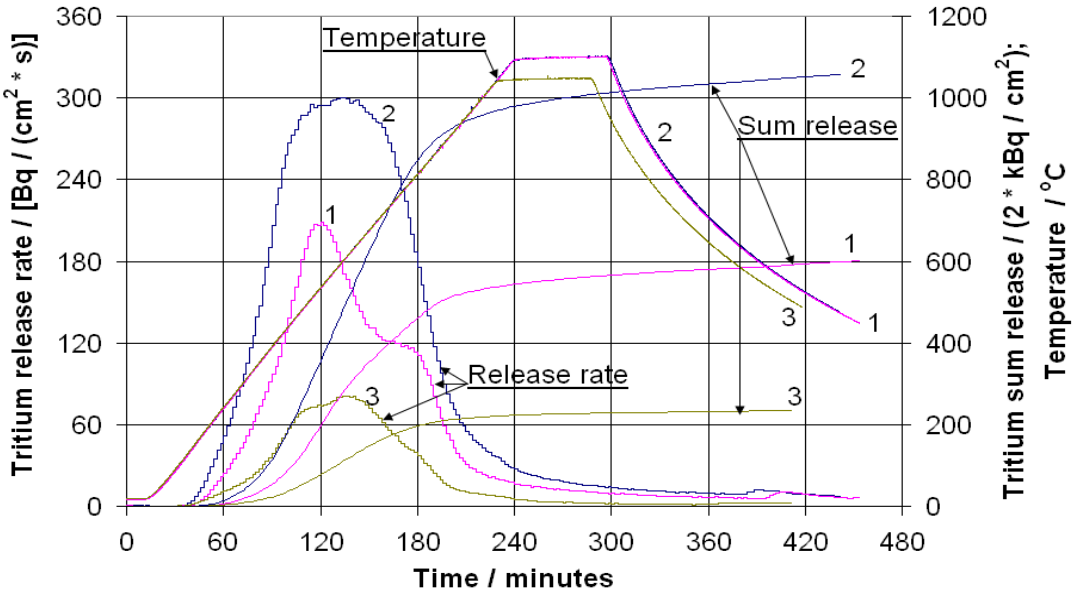

Fig.4.1.8.Tritium release by thermal desorption from the A1 discs of cylinders 1 (1), 4 (2) and 5 (3) of tile 14BWG4B.

4.1.4 Conclusions

1. The tritium profile in the JET divertor SRP 14BWG4B tile is not uniform both as in the poloidal and as in the toroidal direction of the tile.
2. Distribution of tritium in the JET divertor MkII SRP tile show that the largest amount of tritium is accumulated near to the louvers side.
3. For tile 14BWG4B, the plasma-facing surface disks A1 at the louvers (cylinders 10 & 11) have the surface activity of tritium (10-65 MBq/cm2) by a factor of 10-100 higher than that (0.5-2.1 MBq/cm2) at the SRP (cylinders 1-5).
4. Tendency of tritium distribution in depth profiles in the investigated cylinders is similar. Amount of the retained tritium in plasma facing part of the carbon deposited layers is in the range of 10^9 $Bq.g^{-1}$, whereas in the middle part of the cylinder concentration of the tritium sharply decrease and is nearly constant10^5 Bq/g^{-1}, but in the rear side of the cylinder the concentration of tritium slightly increases.
5. Tritium release from plasma exposed surface disks starts at ≤ 200 °C, the release rate reaches a maximum at < 680 °C and decreases rapidly at temperatures above 950 °C.

4.2. Tritium release from the pebble-bed assembly's neutron irradiated beryllium pebbles under action of temperature and tritium of the high dose irradiated beryllium pebbles

Principal investigator: G. Kizane

4.2.1 Introduction

Beryllium pebbles are foreseen as a neutron multiplier to the reference concept of the helium-cooled pebble-bed breeding blanket (HCPB) in the European Breeding Blanket Programme for the DEMO design
The helium-cooled pebble bed (HCPB) is one of the concepts developed in Europe for the breeding blanket of the future DEMO/Power Plant. In the HCPB blanket, beryllium or beryllide pebbles (∅≈1 mm) are used as a neutron multiplier, and Li_4SiO_4 or Li_2TiO_3 ceramic pebbles (∅≈0.4-0.6 mm) are used as a tritium breeder. Under neutron irradiation, helium and tritium are produced in beryllium as a result of neutron-induced transmutations. Helium, being insoluble in metals, precipitates as bubbles in beryllium and causes swelling. Tritium accumulation in beryllium pebbles is a significant safety and waste handling issue of the HCPB blanket. Consider pro able tritium retention may cause an environmental hazard in emergency and problems with utilization of used beryllium. It is not desirable from the viewpoint of economy of tritium. Under the real operating conditions of the HCPB of different designs, the multiplier Be pebbles will be subjected to action of a high temperature up to 920 K or even higher – 700-1050 K or up to 1170 K as given in literature. Tritium release is governed by several mechanisms: diffusion, surface desorption, trapping.
The aim of the programme of the year 2010 was to investigate post irradiation tritium release from pebble bed assembly's (PBA) irradiation experiment beryllium pebbles under action of both temperature ramp and at a constant temperature relatively long time. In the year 2010 laboratory began investigations on tritium behaviour of the HIDOBE-I beryllium pebbles and the first results on the tritium specific activity of pebbles from HIDOBE-I experiments are obtained and given.

4.2.1 Experimental

Samples investigated

Material and irradiation characteristics of the beryllium pebbles irradiated in the PBA, EXOTIC 8-3/13 and BERYLLIUM experiments with fast fission neutrons in HFR are compared in Table 4.2.1. The PBA pebbles have a rather spherical shape with some indentations on a fraction of the pebbles. Optical microscopy of cross sections of the Be pebbles shows that a large fraction of the Be pebbles have a large closed pore of 0.1-0.2 mm in diameter. These large pores are the result of the manufacturing of the pebbles. The pebble density was reported to be >99% of the theoretical density.

Tritium release at annealing

Tritium release experiments were performed in a setup enabling annealing at temperatures up to 1310-1550 K (Fig. 4.2.1). One PBA Be pebble was investigated in each tritium release experiment. The tritium release was performed in a continuous

flow of the purge gas He + 0.1% H_2. The sample temperature was initially increased linearly with time at a constant rate of 2.3-4.8 K/min from room temperature up to an end temperature of 1310-1550 K, which was kept constant for 1 h.

Table 4.2.1. Characteristics of the beryllium pebbles

Irradiation	PBA	EXOTIC 8-3/13	BERYLLIUM
Manufacturer	NGK Insulators Ltd., Handa City, Japan	Brush Wellman Inc., Cleveland, Ohio, USA	Brush Wellman Inc., Cleveland, Ohio, USA
Production process	rotating electrode process	inert gas atomization	fluoride reduction process
Diameter, mm	0.9-1.1	0.1-0.2	Approx. 2
Grain size, μm	40-200	40-200	40-200
Main impurities	2300 ppm BeO, 300 ppm Mg	3400 ppm BeO, 100 ppm Mg	3125 ppm BeO, 1200 ppm Mg
Irradiation time	294 full power days	449.8 days	97.4 days
Neutron fluence (E>0.1 MeV)	$3\text{-}4 \times 10^{25}$ m^{-2}	2.70×10^{25} m^{-2}	1.24×10^{25} m^{-2}
Irradiation temperature	523-773 K	800-900 K	780 K
^{4}He content	300-600 appm ([1])	285 appm ([2])	480 appm ([2])
Year of EOI ([3])	November 2004	2000	1994
Year of TA	2008-2010 ([4])	2008	2005
Total tritium	2-4 GBq/g ([4])	2-20 MBq/g	0.6-1.5 GBq/g
Abundance of T_2	96±3 % ([4])	56±15 %	85±3 %
Abundance of T^0	1±1 % ([4])	32±17 %	10±3 %
Abundance of T^+	3±2 % ([4])	12±3 %	5±1 %

([1]) – He production in Be, ([2]) – calculated on the basis of the irradiation history,
([3]) – EOI – end of irradiation, ([4]) – the present study.

Fig. 4.2.1. Disassembled view of the setup for the tritium release experiments: 1 and 2 – compartments of the quartz tube for the sample and for a bed of granulated zinc respectively; 3 – a porcelain boat for the sample under study; 4 – a white cylindrical ceramic holder for the cold junction of a type S thermocouple of 300 mm in length; 5 – a type K thermocouple to measure the temperature of the cold junction of the type S thermocouple; 6 – a "Nabertherm" RT 50-250/13 tube furnace; 7 – a P 320 controller for the "Nabertherm" tube furnace; 8 – a tube furnace for heating the zinc bed; 9 and 10 – measuring and driving type K thermocouples for the zinc bed respectively; 11 – an ice bath for the cold junctions of type K thermocouples 5 and 9.

4.2.3 Results

Tritium release at temperature ramps

Investigations of the tritium release with the temperature ramps to 1310-1520 K was realized in order to obtain temperature-programmed desorption spectra of tritium from the beryllium pebbles, to get general insight into tritium release properties of the beryllium pebbles. Histograms of the tritium release rate and curves of the tritium sum release from two PBA beryllium pebbles at the given temperature programs including a ramp at 4.8 K/min to 1350 K and anneal at 1373-1525 K for 1 h are given in Fig. 4.2.2.1a. A significant tritium release started at 920 K. Generally, the tritium release took place in a single maximum with two distinct stages – a stage of a gradual increase in the tritium release rate in the temperature range from 920 K to 1178-1223 K, which was a shoulder before a maximum, and a stage starting with an abrupt increase in the tritium release rate and resulting in a maximum at 1253-1287 K. The histograms in the range of the maximum had a fine structure with possible presence of minor peaks. At the temperature above 1327 K, the histograms of the tritium release rate were gradually descending with no apparent transitions at the steps of the temperature program.
Histograms of the tritium release rate and curves of the tritium sum release from four PBA beryllium pebbles at the given temperature programs consisting of a ramp at 2.4 K/min to 1309 K and anneal at 1309-1320 K for 1 h are given in Figs. 4.2.21b and c. A significant tritium release started at 830 K. In Fig. 4.2.2.1b, though both the pebbles had a similar final value of the tritium sum release 2.71-2.75 GBq/g, they had considerably different histograms of the tritium release rate. The PBA Be pebble of 1.22 mg had the histogram with a shoulder at 920-1178 K and a maximum at 1216-1221 K that was qualitatively similar to those at 4.8 K/min given in Fig. 4.2.2.1a. Under the temperature program given in Fig. 4.2.2.1b, four other PBA Be pebbles of 0.96-1.24 mg had tritium release patterns of the final sum release of 2.6-3.0 GBq/g that were qualitatively similar to curve 3 of Fig. 4.2.2.1b – for instance, curves 5 and 6 in Fig. 4.2.2.1c. However, the histogram of the tritium release rate from the 0.87 mg pebble had a distinct maximum at 960-965 K and a distinct set of three peaks at 1028-1064 K resulting in a factor of 2.4 higher tritium sum release at 1178 K than that of the 1.22 mg pebble. The 0.87 mg pebble had a sharper maximum at 1228-1233 K than the 1.22 mg pebble in the temperature range of 1178-1309 K. No significant amounts of residual tritium were found at dissolution of the pebbles in 2 mol/L H_2SO_4 after their annealing under the temperature programs given in Figs. 4.2.2.1a-c. That testifies that a complete release of tritium took place under the given conditions of annealing.

Tritium release at a constant temperature

The experiments at a constant temperature of 1000-1180 K for 4-23 h were carried out with the aim to investigate tritium release properties of the beryllium pebbles at the temperatures related to the operating temperatures of the multiplier Be pebbles in the HCPB blanket. Curves of the tritium release for the lower final anneal temperatures of 1083-1183 K for 4 h are shown in Fig. 4.2.1d. In curves 7 and 8, a transition from the gradual to burst release of tritium at the final anneal temperatures of 1129-1183 K is evident. The time lag of release burst can be determined for curves 7 and 8: about 1 h at 1178 K (curve 7) and about 2.5 h at 1132 K (curve 8).

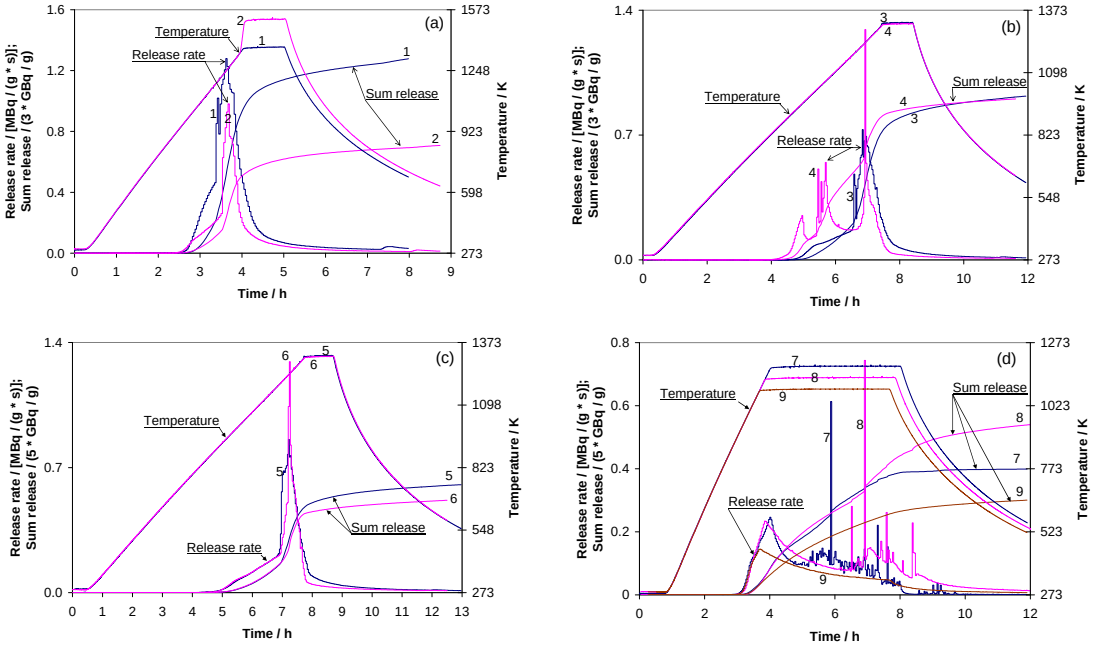

Fig. 4.2.2. Tritium release rate and tritium sum release from the PBA beryllium pebbles heated at the given temperature: curves 1 and 2 – a linear ramp of 4.8 K/min to an anneal temperature of 1373-1525 K; curves 3-6 – a linear ramp of 2.3-2.4 K/min to an anneal temperature of 1308-1320 K; curves 7-9 – a linear ramp of 4.5 K/min to an anneal temperature of 1173-1183 K (curve 7), 1129-1135 K (curve 8) and 1083-1090 K (curve 9). The PBA Be pebbles had the following masses (mg), final values of the tritium sum release for 1 g of the sample (GBq/g) and final values of the tritium fractional sum release (%):1 – 0.86, 3.83, 100%; 2 – 1.61, 2.12, 100%; 3 – 1.22, 2.75, 100%; 4 – 0.87, 2.71, 100%; 5 – 1.12, 3.02, 100%; 6 – 0.98, 2.58, 100%; 7 – 1.13, 2.00, 91.7%; 8 – 0.90, 2.71, 84.5%; 9 – 1.05, 1.50, 56.8%.)

Table 4.2.2. Final values of the tritium sum release from the PBA beryllium pebbles calculated for initial (i) and final (f) backgrounds

Fig.	Mass mg	∅ mm	Background (i) cps	Sum release (i) GBq/g	Background (f) cps	Sum release (f) GBq/g
2a	0.86	0.96	2.72	3.83	91.5	3.34
2a	1.61	1.18	0.37	2.12	63.7	1.81
-[a]	1.23	1.08	2.91	2.48	63.6	2.13
2b	1.22	1.08	2.09	2.75	53.8	2.37
2b	0.87	0.96	2.49	2.71	28.5	2.46
-[b]	1.24	1.09	1.29	2.60	45.4	2.32
2c	1.12	1.05	2.11	3.02	46.4	2.68
-[b]	0.96	1.00	1.74	2.86	45.2	2.49
2c	0.98	1.00	2.26	2.58	40.4	2.18

[a] not shown in Fig. 4.2.2a. [b] not shown in Figs. 4.2.2b or 4.2.2c.

Tritium release from a PBA Be pebble at two identical anneals at 1083-1090 K for 4 h is shown in Fig. 4.2.2a. In the first anneal, tritium release is similar to that of another

PBA pebble shown as curve 9 in Fig. 4.2.2 d. In the second anneal, tritium release may be considered as a continuation of that of the first anneal. After the end of temperature program and cooling down to 968 K, at the experiment time of 8 h, burst release of tritium is evident in curve 2 in Fig. 4.2.2a.
Tritium release from a PBA Be pebble at longer anneal at 1083-1089 K for 7.2 h is shown in Fig. 4.2.2b. Also in this case, burst release of tritium is evident in curve 3 in Fig. 4.2.4.2b after the time of about 6.5 h.
The stages of gradual and burst release are related to the tritium release by atomic diffusion and bubble venting respectively. It is worth noting, as it can be seen in Figs. 4.2.2.d and 4.2.2, that the sharp peaks of burst release are followed by gradually descending curves of tritium release rate that are higher than those before the burst release. That can be explained by the fact that the pores that appeared in the pebble at the burst release increase the outer surface of the pebble and thus increase the rate of the tritium release limited by atomic diffusion from inner part of the pebble.

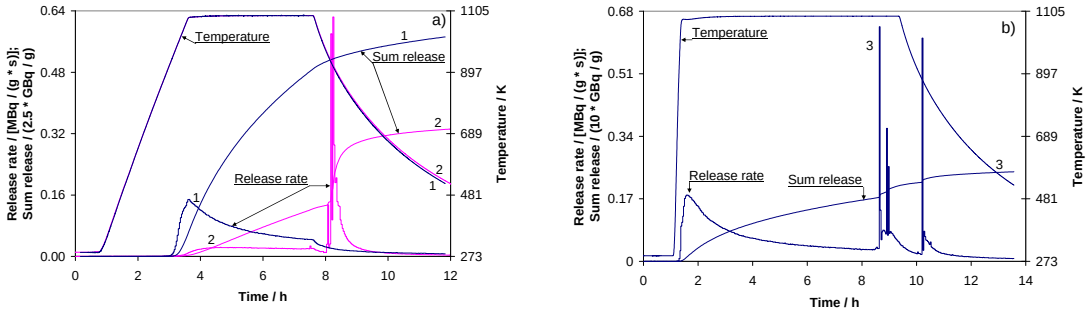

Fig. 4.2.3. Tritium release rate and tritium sum release from two PBA beryllium pebbles heated at the given temperature: curves 1 and 2 – two subsequent linear ramps of 4.5 K/min to an anneal temperature of 1083-1090 K of the same pebble of 1.12 mg; curve 3 – a ramp of up to 34 K/min to an anneal temperature of 1083-1089 K of another pebble of 0.67 mg. The PBA Be pebbles had the following masses (mg), final values of the tritium sum release for 1 g of the sample (GBq/g) and final values of the tritium fractional sum release (%):1 – 1.12, 1.43, 49.2%; 2 – 1.12, 0.83, 28.8%; 3 – 0.67, 2.44, 82.9%.
Tritium release from PBA Be pebbles at even longer anneals at 1045 and 1000 K for 22.4 h is shown in Fig. 4.2.3. The two pebbles investigated under the temperature programmes given in Fig. 4.2.3 had quite different tritium release patterns. One noticeable difference is a higher maximum tritium release rate for the pebble annealed at lover temperature (curve 2) than that at higher temperature (curve 1). At 1045 K, no burst release of tritium took place (curve 1, Fig. 4.2.3). However, after annealing at 1000 K, burst release of tritium took place after cooling down to 560 K (curve 2, Fig. 4.2.3). The pebble annealed at 1000 K (curve 2, Fig. 4.2.3) was not dissolved in acid, but was used for microscopy, where it was found that visible cracks were formed and the porosity started to appear in the pebble.
Degrees of detritiation achieved at the annealing shown in Figs. 4.2.1d, 4.2.2 and 4.2.3 are summarized in Fig. 4.2.4. Data from curve 3 in Fig. 4.2.4.1b is included in Fig. 4.2.4 as the first column at 1313 K for 1 h for comparison. Contributions of the tritium release by atomic diffusion before the burst release and the tritium release after the burst release event are estimated in the total degree of detritiation.

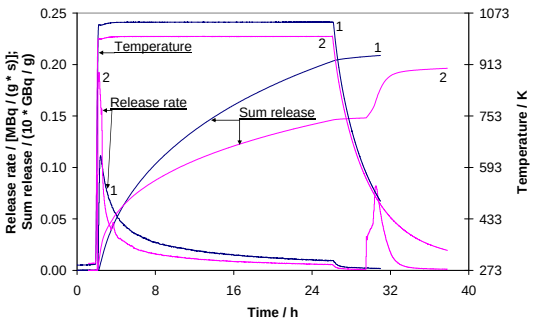

Fig. 4.2.4. Tritium release rate and tritium sum release from the PBA Be pebbles heated at the given temperature: curve 1 – a ramp of up to 36 K/min to an anneal temperature of 1043-1045 K; curve 2 – a ramp of up to 41 K/min to an anneal temperature of 999-1001 K. The PBA Be pebbles had the following masses (mg), final values of the tritium sum release for 1 g of the sample (GBq/g) and final values of the tritium fractional sum release (%):1 – 0.73, 2.09, 74.8%; 2 – 1.21, 1.96, not determined.

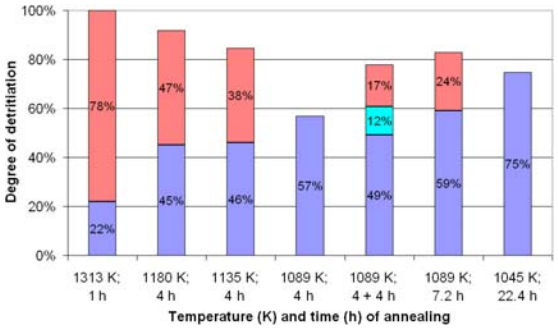

Fig. 4.2.5. Degrees of detritiation of the PBA Be pebbles achieved as a result of annealing under the given temperature and time. Series 1 (periwinkle colour) – the degree of detritiation (22-75%) achieved before the start of the burst release. Series 2 (turquoise colour) - the degree of detritiation (12%) achieved before the start of the burst release in the second annealing. Series 3 (coral colour) – the degree of detritiation (17-78%) achieved after the start of the burst release.

Characterization of the HIDOBE-1 beryllium pebbles

The first experiments on HIDOBE-1 beryllium pebbles were realized. The specific activity of the pebbles was determinate by dissolution technique and is shown in the table 4.2.3.

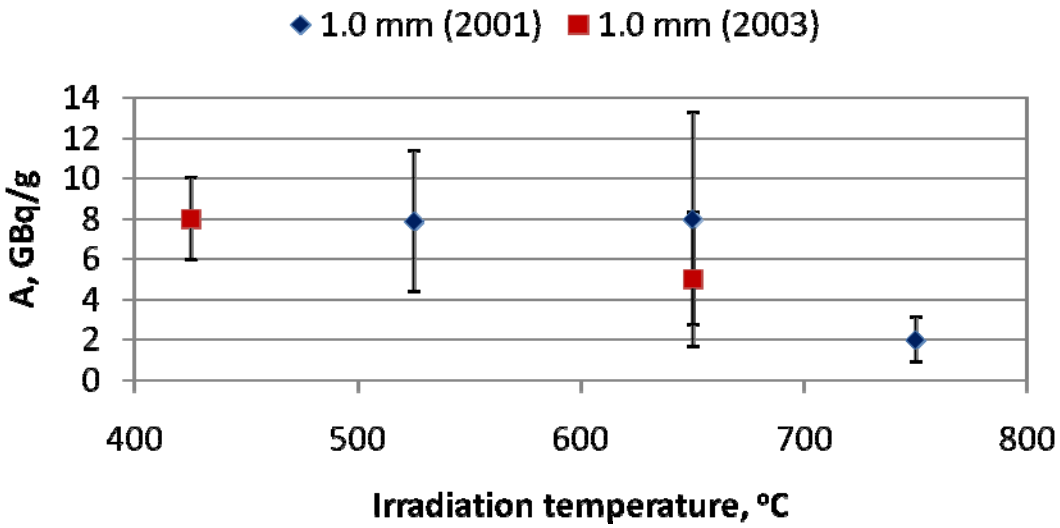

Fig.4.2.6. Tritium mass activity of the HIDOBE-1beryllium pebbles (diameter 1mm, 2001 and 2003) at different irradiation temperatures.

The correlation of tritium amount and irradiation temperature was observed. Tritium mass activity at higher irradiation temperature 750 ^{o}C is 3-4 times less mass activity of tritium than at irradiation temperature 450 ^{o}C (Fig. 4.2.6.).

Table 4.2.3. Mass activity of tritium of the HIDOBE-1 beryllium pebbles

Sample	Irradiation T, ^{o}C	Coding	Number of dissoluted pebbles	Mean, GBq/g	Standard deviation	Mean, GBq/g
1.0 mm(2001)	525	46sPC/3	6	7.0	3.34	8±4
1.0 mm (2001)	650	10sPC/3	2	8.00	0.59	8±5
1.0 mm (2001)	750	9sPC/3	6	1.75	1.05	2±1
1.0 mm (2003)	425	43sPC/3	6	8.31	1.93	
1.0 mm (200)	650	6sPC/3	3	5.28	1.34	5±3
0.5 mm	750	1sPC/3	2	0.38	0.32	1±3

4.2.4 Conclusions

1. Two distinct stages of tritium release – a stage of gradual increase and a stage of abrupt release peaks are evident in the tritium release of the PBA These two stages are related to the tritium release by atomic diffusion and bubble venting respectively.
2. The main maximum of the tritium release rate of the PBA Be pebbles was found to be in the temperature ranges of 1178-1309 K and 1178-1350 K at the temperature ramps of 2.4 and 4.8 K/min respectively.
3. A general trend can be concluded that tritium release from the EXOTIC 8-3/13 pebbles takes place at lower temperatures than that of the PBA and BERYLLIUM pebbles.
4. It can be predicted that increasing the temperature of the beryllium pebble bed at neutron irradiation to from 523-773 K to 1000-1050 K will significantly reduce the tritium inventory in the beryllium pebbles
5. The mass activity of the accumulated tritium in HIDOBE-1 beryllium pebbles correlates with the irradiation temperature.

4.3. Radiolysis of lithium orthosilicate pebbles

Principal investigator: *G.Kizane*

4.3.1 Itroduction

Lithium containing ceramics – silicates and titanates are proposed as breeder blanket components for future fusion reactors in a form of pebbles. One of the technological problems of a fusion reactor is the change in composition and structure of ceramic breeders (Li_4SiO_4 or Li_2TiO_3 pebbles) during long-term operation. In cooperation with Karlsruhe Institute of Technology changes in the composition and microstructure of overstoichiometric Li_4SiO_4 pebbles, fabricated by a melt-spraying process, were investigated after fast electron irradiation.

4.3.2 Experimental

Samples investigated

Three types of pebbles received from the KIT with different diameters and grain sizes were investigated (Table 1). Lithium orthosilicate (Li4SiO4) pebbles were fabricated by a melt-spraying process in a semi-industrial scale facility at Schott AG, Mainz, Germany. In this process the pebble size ranges from about 10 to 1000 μm, but only pebbles with diameters of 250-630 μm are selected for the possible use in the European test blanket module. While larger pebbles crystallize during cooling, pebbles with diameters smaller than 50 μm solidify amorphously. For the experiments, pebbles with a diameter of about 500 μm were annealed to obtain a homogeneous microstructure. Additionally, pebbles of the same fabrication campaign but with diameters of less than 50 μm were heat treated at different temperatures to achieve crystallization and a microstructure with different mean grain sizes. The pebbles were irradiated in quartz tubes in both air and dry argon with accelerated 5 MeV electrons at 560 ±20 K by means of ELU4 accelerator, the dose rate of 24.4 kGy/s. Products of radiolysis were studied by means of FTIR and XRD. TSL and ESR spectroscopy were used to detect radiation defects.

Table 4.3.1. Characteristics of the investigated pebbles

Nr.	Pebble size, μm	Grain size, μm	Annealing temperature, K	Annealing time, h	Excess of SiO_2, wt.%
1.	<50	1	1073	1	2.5
2.	<50	5	1173	128	2.5
3.	500 ±50	10	1243	168	2.5

4.3.3 Results

Analysis of the microstructure of the pebbles at etched cross-sections showed the different grain sizes of the samples before irradiation. In lithium orthosilicate samples 2 and 3 was observed the grains of lithium metasilicate as inter- or intracrystalline inclusions. Because of the small grain size, lithium metasilicate can not be detected in sample 1. In sample 2 the grains seem to be only loosely connected and some of the pebbles were already destroyed during grinding and polishing. This may be caused by

an improper heat treatment during crystallization of the previously amorphous pebbles. After irradiation in air, all samples exhibit a fissured microstructure, and the smaller pebbles (samples 1 and 2) nearly appear to be disintegrated. After irradiation in argon, the samples are nearly unchanged the small pebbles seem to exhibit a slightly more porous microstructure with more gaping grain boundaries, but there is hardly any difference in the microstructure of the large pebbles compared to the unirradiated material. The second phase, lithium metasilicate, can also be detected as inter- or intracrystalline inclusions in samples 2 and 3. Nevertheless, the samples irradiated under air appear to be chemically eroded by possible reactions with air, containing H_2O and CO_2.

ESR spectra of all investigated samples after irradiation with doses up to 10.56 GGy exhibit at least three different lines with g-factors of 2.001, 2.011 and 2.016. Those spectra are similar to previously reported ones for irradiated "pure" Li_4SiO_4 and can be interpreted as superposition of signals from so called E' and HC2 centers (ion radicals SiO_3^{3-} and SiO_4^{3-}, respectively). Ion radical SiO_3^{3-} (HC2 centre) in ESR spectra is presented with 2 lines ($g_{\perp}$=2.009 and $g_{\parallel}$=2.016) due to anisotropy of g-factor. A very week and board multiplex signal was also observed at ESR spectra of irradiated sample 1. This signal can be attributed to electrons localized in anion or oxygen vacancy (so called F^+ centres). ESR spectra of all three samples irradiated in air atmosphere with a dose of 10.56 GGy contain two symmetric lines with 50.2 mT splitting, typical for localized hydrogen atoms. Beside this, several unidentified lines possibly due to impurities were observed at ESR spectra of samples irradiated with a dose of 10.56 GGy in air atmosphere.

Concentrations of stabilized paramagnetic centers in pebbles irradiated with doses from 1 to 5 GGy are in the range of 10^{15}-10^{16} radical/g and slightly increase with increasing absorbed dose. Concentration of free radicals stabilized in samples irradiated in dry argon with absorbed doses of less than 2 GGy are significantly higher than in case of samples irradiated in air atmosphere. For samples irradiated in dry argon an increase of the absorbed dose higher than 5 GGy cause a decrease of radicals' concentration. On the other hand, a surprisingly high concentration of stabilized paramagnetic centers (10^{17}-10^{19} radical/g) was observed in samples irradiated with a dose of 10.56 GGy in air atmosphere.

In irradiated pebbles the same radiation defects are stabilized that were previously detected in "pure" Li_4SiO_4, but the concentration of stabilized free radicals at doses from 1 to 5 GGy is approximately 2 times higher. ESR measurements of "pure" Li_4SiO_4 irradiated with a dose of 10.56 GGy were not made previously.

TSL curves of irradiated pebbles are also similar to previously reported ones for irradiated "pure" Li_4SiO_4 and contain three maxima at temperatures of 395±25, 438±12 and 500±50 K. In the high temperature region the fourth maximum is observed at 612±38 K (see Fig. 4.3.1). The maximum at 500±50 K is unstable and disappears within 60 days after irradiation.

The TSL intensity of samples irradiated in dry argon is significantly higher than in case of samples irradiated in air atmosphere. In TSL curves of pebbles irradiated in argon the intensities of the maximum in the high temperature region (612±38 K) are approximately ten to hundred times higher than intensities of other maxima. This may be due to the high temperature (up to 587 K) of irradiation. Beside this, in case of samples irradiated in argon the intensities of the firsts three maxima (395, 438 and 500 K) strongly decrease with the increasing of absorbed dose, and at the high irradiation doses (D>5GGy) only the fourth maximum (at 612 K) can be observed.

On the other hand in TSL curves of samples irradiated in air atmosphere relatively high intensities of low-temperature peaks (at 400, 440 and 500 K) were observed at dose 10.56 GGy. We think that this effect is caused by high concentration of impurities (Li_2O, LiOH, Li_2CO_3 and other products of radiolysis) in irradiated samples. An explanation of this phenomenon can only be made after further investigation of post-irradiation processes in irradiated overstoichiometric lithium orthosilicate pebbles.

TSL optical spectra of all investigated samples indicate a maximum at 3.5 eV. Only TSL optical spectra of pebbles irradiated with a dose less than 1 GGy have a maximum at 2.9 eV. Both these maxima have previously been observed in TSL and radio-luminescence spectra of “pure” Li_4SiO_4. The luminescence band with the maximum at 3.5 eV is due to exited states of SiO_4^{4-} anions (so called "L-centers".

The origin of the luminescence band with a maximum at 2.9 eV is not yet clear, but it is assumed that it is due to excited states of electrons localized in structure defects (so called "F^+-centers"). Light absorption spectra registered by means of light diffuse refraction spectroscopy have a maximum at 3.0 eves (415 nm).

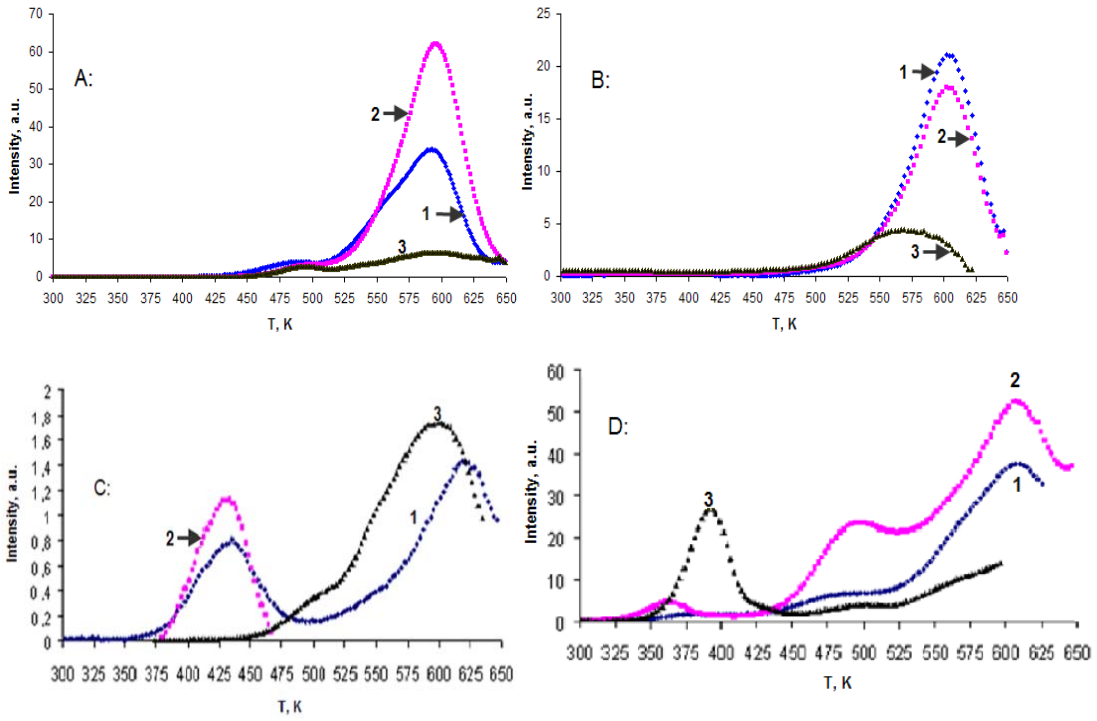

Figure 4.3.1 TSL curves of lithium orthosilicate pebbles after irradiation with doses of 2.64 (A, C) and 10.56 (B, D) GGy in dry argon (A, B) and air (C, D) atmosphere (numbering of curves corresponds to numbers of investigated samples given in table 1). Curve 3.C is decreased 30 times; curve 2.D is decreased 3 times.

Products of radiolysis in irradiated pebbles were investigated by means of XRD and FTIR spectroscopy. Fig. 4.3.2 exemplarily displays the XRD spectra of sample 1 and 3 before and after irradiation at 10.56 GGy. While for sample 3 no change in the phase composition, not even after the irradiation in air could be detected by XRD, the diffraction diagram of sample 1 after irradiation in air exhibits significant amounts of impurities. Due to the large amount of phases, only LiOH, $LiOH \cdot H_2O$ and traces of Li_2CO_3 could be verified, however, traces of lithium oxide cannot be ruled out.

In samples 1 and 2 irradiated in air atmosphere, a significant increase of the initial concentration of Li_2SiO_3 as well as characteristic lines for LiOH and Li_2CO_3 were detected with both mentioned methods. As the specific surface area of samples 1 and2 is 1000 times higher than of sample 3, surface reactions with H_2O and CO_2 are significantly increased in samples with a smaller pebble size. According to FTIR spectroscopy, in all three samples irradiated in air with a dose of 10.56 GGy the concentration of Li_2SiO_3 formed during irradiation is approximately 1 wt% or 4.5 mol%. On the other hand, the concentration of metasilicate in samples irradiated in argon is practically unchanged. Concentrations of colloidal lithium and other reducing products of radiolysis and radiation defects were equal to $4.4*10^{19}$, $1.2*10^{19}$, and $3.1*10^{19}$ electron/g for samples Nr. 1, 2 and 3, respectively. As can be seen from figure 1, the microstructure of pebbles irradiated in argon is virtually identical to the microstructure of the corresponding unirradiated sample (except sample 1, where small changes can be observed).

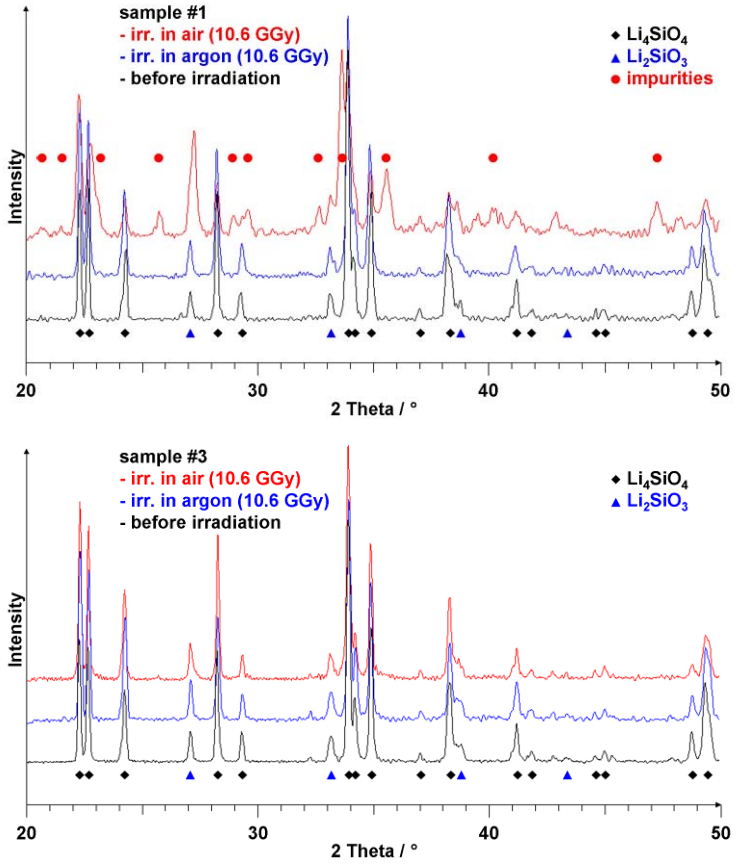

Figure 4.3.2: XRD spectra of sample 1 (top) and sample 3 (below) before and after irradiation with an absorbed dose of 10.56 GGy.

4.3.4 Conclusions

1. The degree of decomposition $\alpha_{10.56}$ of the lithium orthosilicate matrix at an absorbed dose of 10.56 GGy calculated from estimated concentration of radiolytic metasilicate is approximately equal to 1.5% for irradiation in air atmosphere and 0.15% for irradiation in dry argon. This is significantly lower than the value $\alpha_{10.56}\approx5\%$ calculated on base of empiric equation

2. From the comparison of the obtained data for investigated pebbles it can be stated that the pebbles with the larger grain size, but especially the sample 3 with the larger pebble size (500 μm pebbles with a grain size of 10 μm) have a higher radiation stability than sample 1 (<50 μm pebbles with a grain size of only 1 μm)

3. Comparison of the obtained date for the investigated pebbles allow to say that pebbles with a diameter of 500 μm, which represent the potential material for the European test blanket module, have a higher radiation stability than the smaller pebbles.

5. STAFF MOBILITY ACTIONS

5.1. STAFF MOBILITY VISITS

Gunta Kizane	Monitor Meeting Breeder Blanket Be pebbles, Barselona 2-5 Feb, 2010, Kick of Meeting HIDOBE-1, 8-19 Apr, Barselona F4E monitoring meeting, ITER cooperation, 28-30 Apr Barselona 4th Progress Meeting on the GOTP "EUROBREED", 24-27Nov, 2010, Budapest, Hungary General Monitoring Meeting to present the status of work under tasks " JW9-FT-3.46", JW10-FT-3.62" and present an explanation of the background, purpose and objectives of the task JW11-FT-1.19" at the Kick-off Technical meeting. 6Dec–12Dec, 2010, the JET, Culham Science Centre, Abingdon, UK. Oral presentation
Elina Pajuste	CCFE, Culham, Sussex University, Brighton, Got EUROBREEED, mobility 29 days -11.Apr.-9Mai.2010 CCFE, Culham, Sussex University, Brighton, Got EUROBREEED, mobility 29 days -4.-31 Jul.2010 4th Progress Meeting on the GOTP "EUROBREED", 24-27Nov, 2010, Budapest, Hungary
Olgerts Dumbrajs	University of Maryland 31 January – 1 March KIT Karlsruhe, 1 September – 30 September IPP Garching, 1 October – 30 October
Jurijs Zukovskis	KIT, Karlsruhe, 25 May – 5 June KIT, Karlsruhe, 23 October – 7 November
Ivars Tale	IPP, Garching, 20 July – 23 July F4E, Barselona, 20 October – 23 October Wien EFDA Ann. meeting, 2 November – 6 November
Olgerts Lielausis	IST, Portugal, 10 March – 21 March IPP, Garching, 21July - 23 July Wien EFDA Ann. meeting, 2 November – 6 November
Aleksejs Klukins	IST, Portugal, 10 March – 21 March

6. OTHER ACTIVITIES

6.1. Conferences, Workshops and Meetings

Results of fusion research were presented at the conferences:

1. The 26th Scientific Conference of Institute of Solid State Physics. University of Latvia, Riga, February 11-13, 2010.
2. International Baltic Sea Region Conference "Functional Materials and Nanotechnologies 2009" (FM&NT-2009) Riga, 16th –19th March 2010. – Institute of Solid State Physics, University of Latvia.
3. The 52nd international scientific conference of Daugavpils University, Daugavpils, Latvia, April 14 – 17, 2010.
4. 19th International Conference on Plasma Surface Interaction (PSI-19) held in San Diego, USA, May 24-28, 2010.
5. International Workshop on Hydrogen Isotopes in Fusion Reactor Materials held in Pleasanton, USA, May 31- June 1, 2010.
6. The 12th Conference "Advanced Materials and Technologies" European Doctorate in Physics and Chemistry of Advanced Materials." Palanga, Lithuania, August 27 – 31, 2010.
7. 9th International Conference on Tritium Science and Technology "Tritium 2010", Nara, Japan, October 24-29, 2010.

7. PUBLICATIONS 2010

7.1. FUSION PHYSICS AND PLASMA ENGINEERING

7.1.1. Publications in scientific journals

1. O. Dumbrajs, V. Igochine, A. Gude, M. Maraschek, H. Zohm, and ASDEX Upgrade, Temporal evolution of neoclassical tearing modes in the frequently interrupted regime, PHYSICS OF PLASMAS **17**, 042118 2010.
2. O. Dumbrajs, Influence of Possible Reflections on the Operation of European ITER Gyrotrons, J. Infrared Milli Terahz Waves (2010) 31:892–898.
3. O. Dumbrajs and G. S. Nusinovich, To the theory of high-power gyrotrons with uptapered resonators, PHYSICS OF PLASMAS **17**, 053104 2010.
4. V. Igochine, J. Boom, Classen, O. Dumbrajs, S. Günter, K. Lackner, G. Pereverzev, H. Zohm, and ASDEX Upgrade Team, Structure and dynamics of sawteeth crashes in ASDEX Upgrade,PHYSICS OF PLASMAS 17, 122506 2010.
5. A. Gopejenko, Yu.F. Zhukovskii, P.V. Vladimirov, E.A. Kotomin, and A. Möslang, *Ab initio* simulation of yttrium oxide nanocluster formation on *fcc* Fe lattice. - *J. Nucl. Mater.*, 2010, 406, p. 345–350.

7.1.2. Conference articles

1. A. Gopejenko, Yu.F. Zhukovskii, P.V. Vladimirov, E.A. Kotomin and A. Möslang, "Y, O and Fe vacancy defect complex modeling in *fcc* Fe lattice". 26th ISSP Conference (Riga, Latvia, February, 2010), Abstracts: p. 30.
2. A. Gopejenko, Yu.F. Zhukovskii, P.V. Vladimirov, E.A. Kotomin, and A. Möslang, "*Ab initio* calculations of yttrium and vacancy point defects for ODS steels

modeling". 7th International conference "Functional materials and nanotechnologies" FMNT-2010 (Riga, Latvia, March, 2010), Abstracts: p. 182.

3. A. Gopejenko, Yu.F. Zhukovskii, P.V. Vladimirov, E.A. Kotomin, and A. Möslang, "Simulation of yttrium oxide particle formation in iron in support of ODS steel development". 8th International Conference "Information Technologies and Management", IT&M'2010 (Riga, Latvia, April, 2010), Abstracts: p. 20-21.

4. A. Gopejenko, Yu.F. Zhukovskii, P.V. Vladimirov, E.A. Kotomin, and A. Möslang, „Pair and triple point defect complex modeling in *fcc* Fe lattice". Spring European Materials Research Society (E-MRS) Meeting (Strasbourg, France, June, 2010), Abstracts: NPVI-13.

5. Gomes R.B., Silva C., Fernandes H., Duarte P., Lielausis O., Klykin A., Platacis E. Dynamic behavior of a Liquid Gallium Jet under the influence of the Tokamak ISTTOK Plasmas; 19 Internat. Conf. on Plasma Surface Interaction., P2-83, May 24-28 (2010) Sam Diego, USA.

7.2. FUSION TECHNOLOGY

7.2.1. Publications in scientific journals

1. E. Pajuste,A. Vitins,G. Kizane,V. Zubkovs and P. Birjukovs Tritium distribution and chemical forms in the irradiated beryllium pebbles before and after thermoannealing. *Fusion Engineering and Design*. *In Press, Corrected Proof*, *Available online 16 March 2011.*

2. E. Pajuste,A. Vitins,G. Kizane,V. Zubkovs and P. Birjukovs Tritium distribution and chemical forms in the irradiated beryllium pebbles before and after thermoannealing. *Fusion Engineering and Design*. *In Press, Corrected Proof*, *Available online 16 March 2011.*

ACCEPTED

1.Vītiņš,V. Zubkovs,G. Ķizāne,E. Pajuste and V. Kinerte Tritium release characteristics of neutron-irradiated reference beryllium pebbles for the helium cooled pebble bed (HCPB) blanket. *Fusion Science and Technology*, (Special Issue for TRITIUM2010), provisionally accepted.

2. Vītiņš,V. Zubkovs,G. Ķizāne,E. Pajuste and V. Kinerte Tritium release characteristics of neutron-irradiated reference beryllium pebbles for the helium cooled pebble bed (HCPB) blanket. *Fusion Science and Technology*, (Special Issue for TRITIUM2010), provisionally accepted.